Enzymatic Biodegradability of Pristine and Functionalized Transition Metal Dichalcogenide MoS 2 Nanosheets

Rajendra Kurapati, Laura Muzi, Aritz Perez Ruiz de Garibay, Julie Russier, Damien Voiry, Isabella A Vacchi, Manish Chhowalla, Alberto Bianco

Enzymatic biodegradability of pristine and functionalized transition metal dichalcogenide MoS_2 nanosheets

*Rajendra Kurapati, Laura Muzi, Aritz Perez Ruiz de Garibay, Julie Russier, Damien Voiry, Isabella A. Vacchi, Manish Chhowalla and Alberto Bianco**

Dr. Rajendra Kurapati, Dr. Laura Muzi, Dr. Aritz Perez Ruiz de Garibay, Dr. Julie Russier, Miss Isabella A. Vacchi, Dr. Alberto Bianco
CNRS, Institut de Biologie Moléculaire et Cellulaire, Laboratoire d'Immunopathologie et Chimie Thérapeutique, 15 rue René Descartes, 67000 Strasbourg, France
E-mail : a.bianco@ibmc-cnrs.unistra.fr
Dr. Damien Voiry[#], Prof. Dr. Manish Chhowalla
Materials Science and Engineering, Rutgers - The State University of New Jersey, 607 Taylor Road, Piscataway, New Jersey 08854, USA
[#]Present address : IEM (Institut Européen des Membranes), UMR 5635, Université de Montpellier, CNRS, ENSCM, F-34095, Montpellier, France

Keywords: molybdenum disulfide, graphene related materials, degradation, peroxidases, cytotoxicity

2D transition metal dichalcogenide MoS_2 nanosheets are increasingly attracting interests due to their promising applications in materials science and biomedicine. However, their biocompatibility and their biodegradability have not been thoroughly studied yet. Here, we investigated the biodegradability of exfoliated pristine and covalently functionalized MoS_2 (*f*-MoS_2). First, biodegradability of these nanomaterials was evaluated using plant horseradish peroxidase and human myeloperoxidase. The results revealed that the enzymatic degradability rate of MoS_2 and *f*-MoS_2 was slower than in the case of the simple treatment with H_2O_2 alone. In parallel, high biocompatibility of both pristine and *f*-MoS_2 nanosheets was found up to 100 µg mL^{-1} both in cell lines (HeLa and Raw264.7) and primary immune cells. In addition, no immune cell activation and minimal pro-inflammatory cytokine release were observed in RAW264.7 and human monocyte-derived macrophages, suggesting a negligible cellular impact of such materials. Furthermore, the effects of degraded MoS_2 and partially degraded *f*-MoS_2 products on cell viability and activation were studied in cancer and immune cells. A certain cytotoxicity was measured at the highest concentrations. Finally, to prove that the

cellular impact was due to cell uptake, we assessed the internalization of both pristine and functionalized MoS_2 in cancer and primary immune cells.

1. Introduction

Two dimensional transition metal dichalcogenides (TMDCs) like MoS_2 are the second most studied layered materials after graphene.[1] TMDCs have unique physicochemical properties, thus attracting enormous interest for the next generation of electronic and optoelectronic devices, for catalysis, for sensing, for energy storage, etc.[1-2] Related to these applications, there is a serious concern about the stability or degradability of TMDCs in air and aqueous media. Indeed, the stability of such nanomaterials can influence their behavior in the different types of envisaged uses.[3-5] MoS_2 is considered relatively chemically inert in ambient conditions. However, its chemical stability, optical and electrical properties are dependent on its crystalline phase. The most common crystalline phase of MoS_2 is the trigonal prismatic (2H phase). In this phase, MoS_2 acts as semiconductor, while in the orthogonal phase (1T phase) MoS_2 acts as metal.[6] MoS_2 in 1T phase is more reactive than in 2H phase, the latter being inert towards most of the chemicals. Indeed, the difference in their electronic states dictates the chemical reactivity of these two crystalline forms of MoS_2. Although metastable, it has been shown that 1T phase of MoS_2 can be stabilized by insertion of Li^+ ions into its crystal lattice, and recently covalent functionalization can also stabilize this phase.[7] Earlier, Voiry *et al.* reported a simple and efficient route for covalent functionalization of MoS_2 sheets facilitated by electron transfer between electron rich metallic 1T phase and organohalides leading to semiconducting MoS_2.[7] Covalent functionalization of MoS_2 sheets was also achieved by exploiting the reactivity of surface and edge defects.[8] The defects on the lattice of MoS_2 were modified, for example, by functionalization with thiols leading to MoS_2 sheets with tuned electronic properties.[8] Alternatively, electron transfer characteristics of MoS_2 can be altered by complexation between MoS_2 layers and optoelectronically active molecules like phthalocyanines.[9]

Besides the development for electronics, optoelectronics and catalytic applications, to mention few of them, biomedical applications of exfoliated TMDCs are increasingly attracting the attention as promising alternatives to graphene. This is mainly due to their high biocompatibility compared to other nanomaterials and strong contrast properties because of the presence of heavy elements like Mo, W, Bi, etc.[3] In this context, TMDCs showed high potential in drug delivery, cancer theranostics, antimicrobials, bioimaging and biosensing.[3, 10-12] Near-infrared light mediated multimodal cancer theranostics based on TMDCs seems to be more promising for biomedicine due to higher photothermal conversion ability as well as stronger contrasting nature over carbon nanomaterials.[3] However, a limited number of data on toxicity are available, while the enzymatic degradability of TMDCs has not been studied yet.[13-14] A few studies showed that MoS_2 displays better biocompatibility than graphene or graphene oxide, but this needs to be confirmed by further works.[15-17] A recent study demonstrated that the cytotoxicity of MoS_2 depends of its aggregation state [15] and the extent of exfoliation.[13] Highly dispersed MoS_2 sheets were not cytotoxic compared to aggregated sheets, while highly exfoliated sheets induced higher cell mortality compared to moderately exfoliated sheets.[13] From a clinical point of view, any nanomaterials, either as vehicle to carry therapeutic molecules or as implanted material in regenerative medicine, should be excreted from the body or biodegraded.[18]

It is known that MoS_2 can be decomposed in the presence of H_2O_2.[19] Since, hydrogen peroxide is a ubiquitous molecule, we thought that it could be interesting to evaluate the decomposition or degradation of MoS_2 sheets at physiological concentrations of H_2O_2. On the other hand, an increased secretion of reactive oxygen species (ROS) including superoxide ($O_2^{\cdot -}$), hydroxy radicals ($HO^{\cdot}$) and hydrogen peroxide occurs in cancer tissues or in inflammatory conditions.[20-22] High amounts of ROS are caused by oncogene stimulation, malfunction of mitochondria and chronic inflammation.[22] ROS affect the proteins which control the redox balance, leading to high production of H_2O_2.[20, 22] The concentration of ROS

in tumor cells is approximately 100 times more than in normal cells.[23] Since 50 to 100 μM of H_2O_2 concentration are more biologically relevant concentration, H_2O_2-responsive anticancer drug delivery systems have been recently designed. [24-26] In this context, we considered important to study the stability of MoS_2 sheets under similar oxidative conditions to reveal their potential as biodegradable nanocarriers for drug delivery applications.

Having in mind the possibility to extend the use of TMDC materials in biomedicine, we have thus decided to investigate the biocompatibility and biodegradability of MoS_2. For this purpose, we have selected two types of highly water dispersible MoS_2 samples, namely metastable pristine MoS_2 and covalently functionalized and highly stable *f*-MoS_2, respectively.[7] We started to evaluate the biodegradation of MoS_2 materials by model peroxidase enzyme horseradish peroxidase (HRP), human myeloperoxidase (MPO), and by hydrogen peroxide alone. We then studied the cytotoxicity of these materials using two different cell lines and primary immune cells (hMDMs, human monocyte-derived macrophages). We used HeLa cells as both epithelial and cancer cell model and RAW 264.7 macrophages as immune and phagocytic model. hMDMs were obtained from PBMCs from healthy donors and used to address the overall effect of MoS_2 and *f*-MoS_2 towards primary immune cells. We carried out cell viability and pro-inflammatory activation tests to measure key cytotoxicity parameters. Then, we studied the cytotoxicity of byproducts obtained during the process of biodegradation of MoS_2 and *f*-MoS_2 using hydrogen peroxide. Finally, we analyzed the uptake of these two materials in cultured cells, and characterized the membrane interaction and the intracellular presence of pristine and *f*-MoS_2 using transmission electron microscopy (TEM). Overall, this report provides a full comprehensive study on cytotoxicity, biodegradability and impact of degradation byproducts of pristine and functionalized MoS_2.

2. Results and discussion

Biodegradation of carbon-based materials was demonstrated by treating them with different types of peroxidases and oxidative enzymes in the presence of low concentration of hydrogen

peroxide.[27-32] More recently we have shown that even 2D materials like hexagonal boron nitride (hBN) nanosheets undergo enzymatic degradation.[33] Unlike graphene and hBN, layered MoS_2 is an unstable material in ambient conditions (room temperature and atmospheric pressure). In fact, it has been shown that MoS_2 is subjected to environmental degradation over a period of several months.[4] The slow oxidation of MoS_2 sheets was observed in the presence of moisture and oxygen.[4] In this direction, we believe that it is very important to study the biodegradability of such sensitive MoS_2 sheets under physiological conditions using different peroxidases and biological concentrations of H_2O_2 to assess possible issues related to biopersistence of this type of 2D materials. Thus, we investigate the capacity of different oxidative enzymes to degrade pristine MoS_2 and MoS_2 covalently functionalized with acetamide groups (*f*-MoS_2). Pristine MoS_2 nanosheets and acetamide *f*-MoS_2 (**Figure S1A** and **B**) were synthesized and characterized according to our previous work.[7] Pristine MoS_2 sheets containing a large fraction of electron rich 1T phase crystals were synthesized by chemical exfoliation and the covalent functionalization of MoS_2 was subsequently obtained by treating MoS_2 with 2-iodoacetamide (see the Supporting Information for details about the synthesis and characterization of MoS_2 and *f*-MoS_2 nanosheets, **Figure S1C-H**).[7] The functional groups were covalently bound to the S atoms [via S-C bond formation, confirmed by X-ray photoelectron spectroscopy (XPS) analyses, **Figure S1**] transforming the metallic phase of MoS_2 sheets into semiconducting state.[7] Pristine and *f*-MoS_2 were characterized by additional techniques including STEM, TEM and Raman (**Figure S1** and **S2**). Both types of MoS_2 possess excellent colloidal stability in water, as supported by the values of their zeta potentials, corresponding to -47 mV for MoS_2 and -43.6 mV for *f*-MoS_2 at pH 7, respectively. Following the synthesis and characterization, we treated these nanomaterials with horseradish peroxidase, myeloperoxidase, or with only biological concentrations of hydrogen peroxide.

2.1. Degradation by HRP

To assess the oxidative effect of peroxidases, pristine and *f*-MoS_2 at 100 µg mL^{-1} were first incubated with HRP in phosphate saline buffer (PBS). H_2O_2 was added (to the final concentration of 40 µM) to both suspensions once per day up to 30 days. The dilution of the samples into PBS initially transformed the stable colloidal water suspensions into blackish aggregated suspensions (**Figure S3A** and **S3E**). After 20 days these suspensions turned into pale brownish in the case of pristine MoS_2 (**Figure S3C**), while it remained still blackish for *f*-MoS_2 (**Figure S3G**). Surprisingly, the color of both MoS_2 and *f*-MoS_2 control samples treated only with H_2O_2, became nearly translucent after 20 days (**Figure S3D** and **S3H)**. We decided then to employ TEM to get more insights about the degradation process. As shown in **Figure 1B** and **1E**, both MoS_2 and *f*-MoS_2 sheets were only partially degraded after 20 day treatment in comparison to the starting materials (**Figure 1A** and **1D**). The control samples treated only with H_2O_2 were instead almost completely degraded in the same period leading to the formation of spherical nanoparticles with size varied from ~20 to 50 nm (**Figure 1C** and **1F**). However, in the case of *f*-MoS_2 we could still observe the presence of some partially degraded nanosheets (**Figure 1F**, inset). Overall, the treatment with HRP/H_2O_2 revealed that the degradation of both MoS_2 nanosheets is completely different from carbon nanomaterials, where nearly full degradation (transparent solutions) was observed using HRP.[29, 34-35] Interestingly, the treatment with H_2O_2 resulted in the complete decomposition of MoS_2 or *f*-MoS_2 nanosheets into nanoparticles, opposite to the results with carbon nanomaterials, where H_2O_2 did not affect their morphology.[28, 30, 34] In addition, we observed that functionalized MoS_2 was degraded more slowly than pristine material, likely due to the stabilization of the latter by covalent functionalization.[7]

2.2. Degradation by hMPO

In the next step, both MoS_2 and *f*-MoS_2 samples at 100 µg/mL were treated with human MPO, an enzyme overexpressed in activated immune cells (e.g. neutrophils), in the presence of NaCl and H_2O_2. In this case, H_2O_2 was added to a final concentration of 200 µM every hour

up to 24 h. The color of pristine MoS_2 suspension changed to nearly translucent after treating with the enzyme for 24 h (**Figure S4**, left vials). However, the decomposition of MoS_2 occurred already after 15 h treatment with only H_2O_2. *f*-MoS_2 suspension also changed to nearly clear solution after treatment with MPO/H_2O_2/NaCl for 24 h (**Figure S4**, right vials). Again a quick decomposition of *f*-MoS_2 leading to an almost clear solution occurred by treating with only H_2O_2 after 15 h. TEM analyses was performed to obtain more details about the morphology of MoS_2 and *f*-MoS_2 remaining materials after the treatment with MPO. Pristine MoS_2 sheets were completely decomposed into tiny fragments after 24 h (**Figure 2B)**. In addition, the layered-like morphology of MoS_2 was entirely lost after treating with only H_2O_2 for 15 h (**Figure 2C**). Similarly, most of the *f*-MoS_2 sheets were also broken down into small fragments and partially degraded sheets (**Figure 2E**) after treatment with the enzyme. Mostly nanoparticles were instead resulted from the treatment with H_2O_2 for 20 h (**Figure 2F**). Overall, TEM results revealed that the degradation of both MoS_2 samples was slowed down in the case of MPO/NaCl/H_2O_2 compared to the treatment with H_2O_2 alone. This is in agreement with the results obtained with HRP. In addition, covalently functionalized nanosheets displayed a higher stability compared to pristine MoS_2 sheets in both enzymatic process using HRP and MPO (**Figure 1** and **2**).

2.3. Degradation by hydrogen peroxide

After proving a direct impact of hydrogen peroxide on the degradation process of MoS_2 and *f*-MoS_2 (**Figure 1** and **2**), we have decided to investigate the stability of both materials in the presence of various concentrations of H_2O_2. Earlier studies revealed that MoS_2 is very sensitive to H_2O_2. Thus, we treated MoS_2 and *f*-MoS_2 sheets with H_2O_2 (added only once at day 0 and incubated for 30 days at 37 ^oC, see Supporting Information for details) varying the concentration from 10 µM to 2 mM. These concentrations correspond to the amount found in normal or physiological altered cells and tissues. Indeed, metabolic activity of cancer cells and activated immune cells produce high amounts of ROS, especially H_2O_2.[24, 26, 36] Our

results revealed a concentration- and time-dependent decomposition of pristine MoS_2 (**Figure S5)**, since the black color of MoS_2 suspensions gradually disappeared by increasing the concentration of H_2O_2 as well as the time. As displayed in **Figure S5**, MoS_2 suspension almost turned into colorless by 14 day treatment even with low concentration of H_2O_2 (10 µM). Surprisingly, MoS_2 sheets slowly decomposed also in PBS. In line with this finding, very recently a study has revealed that MoS_2 materials are unstable and undergoes oxidative dissolutions in simply air-saturated solutions.[37-38] On other hand, *f*-MoS_2 showed greater stability in H_2O_2 compared to the pristine MoS_2 (**Figure S6)**. Also in this case there was a concentration- and time-dependent decomposition. However, this was much slower compared to pristine MoS_2. Even after 30 days, *f*-MoS_2 suspension did not change completely the color. In addition, the stability of *f*-MoS_2 in PBS was much higher. As most of the metastatic cancer cells contains H_2O_2 at concentrations between 50 and 100 µM,[24, 26] we decided to analyzed both pristine and functionalized MoS_2 samples at 50 µM of H_2O_2 of up to 30 days (**Figure S7**). TEM analyses indicated that pristine MoS_2 sheets decomposed nearly completely by 14 day incubation (**Figure 3A** and **3B**), where mostly nanoparticles were observed (**Figure 3B**) along with some partially degraded sheets (**Figure 3A**). In contrast, *f*-MoS_2 sheets were degraded only partially even after 30 days in contrast to pristine MoS_2 (**Figure 3C** and **3D**). The original black color of the solution was not significantly lost supporting the partial degradation and revealing higher stability to oxidation of functionalized MoS_2 sheets (**Figure S7**). Additional TEM images confirming the clear changes in the morphology of the two MoS_2 nanomaterials from 0 to 30 days are shown in **Figure S8**.

To extend the TEM analysis, we carried out high resolution TEM (HRTEM) and selected area electron diffraction (SAED) studies to get more information about the morphological changes and crystallinity of both types of MoS_2 after treating with H_2O_2 for 30 and 60 days, respectively. HRTEM analyses revealed that 30 day-treatment resulted into the transformation of pristine MoS_2 sheets into spherical nanoparticles of size between 5 and 30 nm (**Figure S9A**

and **9B**). In addition, those nanoparticles are in polycrystalline state as measured by SAED analysis (**Figure S9C** and S**9D**). Contrarily, degradation of *f*-MoS_2 sheets did not generate nanoparticles after 30 days (**Figure S10A**), while a few fragments in the nanoscale range were observed after 60 days treatment (**Figure S10B**), along with partially degraded and unmodified sheets (**Figure S10C**). In addition, SAED pattern revealed that the remaining nanosheets (**Figure S10C**) were single crystalline (**Figure S10D**) and the resulted fragments were in amorphous state (**Figure S10F**). Overall, TEM and HRTEM studies indicate that pristine MoS_2 sheets are highly sensitive to H_2O_2, while functionalized MoS_2 are more resistant. We have then checked the cytotoxic effects of the degraded products of MoS_2 and partially degraded *f*-MoS_2 after treating with 50 µM of H_2O_2 for 14 days and 30 days, respectively (*vide infra*).

2.4. Raman analysis

To complement the electron microscopy results, we used Raman spectroscopy to understand the changes in the structure of MoS_2 and *f*-MoS_2 before and after the treatments with HRP, MPO and hydrogen peroxide. TMDCs have two main Raman modes, corresponding to in-plane (E^1_{2g} at 386 cm^{-1}) and out-of-plane (A_{1g} at ~ 406 cm^{-1}) vibrations.[11] In addition, J_1, J_2 and J_3 relative to the vibrations from S atoms are also present. J_1, J_2 and J_3 are identified at ~147, 223 and 328 cm^{-1}, respectively, as displayed in **Figure 4A** (HRP 0 day).[7, 39] The covalent functionalization clearly affected the Raman modes of MoS_2, since J_1 was split into two signals with a new peak at 167 cm^{-1}, and J_2 and J_3 strongly raised in relative intensity (**Figure 4B**, HRP 0 day). These changes are due to the covalent functionalization, where acetamide functional groups are bound to S atoms.[7] Significant changes were observed for pristine sample treated with HRP/H_2O_2 for 30 days, where J_2 peak became negligible and the intensity of J_1 and J_3 was reduced. Importantly, the intensities of both fundamental vibrations of MoS_2 (E^1_{2g} and A_{1g}) also diminished. These fundamental peaks were both missing after treatment with only H_2O_2 for 30 days (**Figure 4A**). In addition, J_2 and J_3 were completely

absent, and a very broad signal was observed at 250-300 cm^{-1}, attributed to Mo-O-Mo deformation in MoO_3.[40-43] The absence of the fundamental peaks revealed that the lattice of MoS_2 crystals was strongly affected. Only a reduction of the intensities of these peaks was instead observed for *f*-MoS_2 treated with only H_2O_2 after 30 days (**Figure 4B)**. *f*-MoS_2 sheets showed a moderate reduction in the intensities of Raman signals in the presence of the enzyme compared to 0 day, confirming the higher stability of functionalized MoS_2 towards HRP/H_2O_2 treatment. As J_1, J_2 and J_3 signals were related to the vibrations from S atoms,[39] the absence of these peaks after treating with H_2O_2, particularly for pristine material, could be due to the formation of MoO_3 as reported earlier for MoO_3 nanoparticles. [43]

In the case of the treatment of MoS_2 and *f*-MoS_2 with MPO/H_2O_2, the intensities of E^1_{2g} and A_{1g} gradually decreased (**Figure 5**). The Raman signatures for both MoS_2 samples are very week after 24 h, (see baseline corrected Raman spectra in **Figure S11** and **S12**), confirming that degradation by hMPO was nearly completed. In the case of H_2O_2 alone treatment, the peroxide caused a higher damage to MoS_2 and *f*-MoS_2 compared to the control sample for HRP. Indeed, 200 µM concentration of H_2O_2 was added every hour for 24 h in the control sample of MPO, while only 40 µM of H_2O_2 was added every day for 30 days in the control sample of HRP. We would like to underline that the vibrations relative to S atoms are absent, likely confirming the formation of oxygenated species.[44]

In the third case corresponding to degradation using increasing concentrations of H_2O_2, we observed the changes in the Raman spectra after the treatment for 30 days (**Figure 6A** and **6B)**. In the case of pristine MoS_2, the intensities of fundamental vibrations (E^1_{2g} and A_{1g}) are reduced gradually by increasing the concentrations of H_2O_2. Again, a broad peak around 250-300 cm^{-1} corresponding to Mo-O-Mo deformation appeared.[40-43] At the same time, also vibrations relative to S atoms gradually diminished. At the highest concentrations, these peaks were completely absent, confirming the complete oxidation of MoS_2. The disappearance of J_1, J_2 and J_3 were not seen for *f*-MoS_2, while a general gradual reduction in the intensities of the

bands was observed (**Figure 6B**). These results strongly confirmed the higher stability of functionalized MoS_2, as already observed by TEM (**Figure 3**).

2.5 X-ray photoelectron spectroscopy analysis

To get more details about the degree of oxidation of molybdenum during the degradation process, XPS analyses were conducted after treating the samples with HRP (30 d), hMPO (24 h) and H_2O_2 alone (14 for MoS_2 and 30 d for *f*-MoS_2, respectively) (**Figure 7** and **S13**). In all conditions, a complete oxidation of Mo(IV) in the pristine MoS_2 into Mo(VI) was confirmed by the presence of Mo^{VI} $3d_{3/2}$ (~236.5 eV) and Mo^{VI} $3d_{5/2}$ (~233 eV) in the Mo 3d high resolution spectra (**Figure 7A**, **7C** and **7E**). In the case of *f*-MoS_2, the presence of mixture of Mo^{VI} 3d and Mo^{IV} 3d revealed instead an incomplete oxidation of *f*-MoS_2 sheets (**Figure 7B**, **7D** and **7F**). We would like to underline that in the starting MoS_2 and *f*-MoS_2, Mo^{VI} 3d peaks are absent (**Figure S1**). The XPS results support also a higher resistance to oxidation of covalently functionalized MoS_2 compared to pristine sheets, in good agreement with Raman and TEM data. In addition, oxidation of S^{2-} into SO_4^{2-} was confirmed by XPS (**Figure S13**). The peak at ~168.5 eV corresponds to S 2p of SO_4^{2-} ions, and the two peaks at ~161 and ~162 are attributed to the binding energies of S 2p (S^{2-} $2p_{1/2}$ and S^{2-} $2p_{3/2}$, respectively) of MoS_2.[45] Sulfur atoms of pristine MoS_2 were oxidized to SO_4^{2-} ions, whereas in the cases of *f*-MoS_2, the mixture of S^{2-} and SO_4^{2-} were observed, as expected due to the incomplete oxidation of *f*-MoS_2 sheets.

2.6. Mechanism of degradation

The degradation trends of MoS_2 and *f*-MoS_2 by HRP, hMPO and H_2O_2 revealed that pristine MoS_2 is the most unstable in the aqueous solution. MoS_2 was even degraded in the PBS within 3 week incubation (see **Figure S5**). The degradation of pristine MoS_2 was faster in the presence of H_2O_2 compared to the treatment with HRP or hMPO, due to a quick oxidation of Mo(IV) into Mo(VI), most likely in the form of MoO_3 or MoO_4^{2-} ions.[19, 46-47] The broad peak that we observed around 250-300 cm^{-1} (centred at ~270 cm^{-1}) in the Raman spectra of pristine MoS_2 treated with HPR and H_2O_2 alone (**Figure 4** and **6**) corresponds to MoO_3 as described in the literature.[40-43] Indeed, it is well known that MoS_2 is oxidized to MoO_3 when treated with hydrogen peroxide.[46] However, in the case of hMPO, which involve different oxidative intermediates (i.e. HOCl), the degradation process likely forms soluble MoO_4^{2-} ions.[38, 47]

Raman (**Figure 4-6**) and XPS analyses (**Figure 7**) confirmed that the degradation of MoS_2 lead the oxidation of molybdenum either into MoO_3 or soluble MoO_4^{2-} ions along with formation of SO_4^{2-} (see the corresponding equations in Supporting Information).[46, 48] Data in the literature further indicate that 1T phase of MoS_2 is metastable due to the richness in electrons, and it can be easily oxidized in the presence of salts, H_2O_2, oxygen and moisture.[4, 19, 38, 49] In addition, a more recent study also suggested that MoS_2 nanosheets can be transformed into soluble MoO_4^{2-} species in a mice model. This study is of particular interest in the context of biomedical applications of TDCMs. Indeed, the authors have demonstrated that the degradation of MoS_2 functionalized with polyethylene glycol (PEG) leads to an enhanced elimination rate *in vivo*. The degradation was confirmed by the generation of MoO_4^{2-} that was excreted within 30 days.[47] In view of the fast oxidation process found in our conditions, it will be also warrant to study *in vivo* degradation of our MoS_2 material. Raman analyses of MoS_2 nanosheets confirmed the presence of Mo-O bonds and the disappearance of the fundamental MoS_2 vibrations (E^1_{2g} and A_{1g}) after treating with H_2O_2 and MPO. In the case of MPO treatment, there is generation of HOCl along with MPO reactive intermediates, which are highly oxidants compared to reactive intermediates of HRP.[27-28] The chemical functionalization stabilized 1T phase of MoS_2 by converting the metallic character into the semiconductor state.[7] The degradation results of *f*-MoS_2 with HRP, MPO and H_2O_2 revealed that the degradation was much slower when compared with pristine MoS_2, as confirmed by XPS analyses.

TMDCs are compounds different from carbon nanomaterials, and the degradation profile of MoS_2 nanosheets results different.[29, 34, 50] Carbon nanomaterials are completely oxidized by reactive intermediates of HRP or MPO whereas MoS_2 materials were more resistant. In contrast, MoS_2 samples are quickly degraded by H_2O_2. We expect that these materials could have different behavior during their interaction with body fluids or peroxidase enzymes and ROS under inflammation conditions. These materials may also have different fate compared

to carbon materials, since they showed to be degraded even in the presence of moisture, salts and ROS. In the next sections, we assess the impact of both pristine and *f*-MoS_2 on various cell lines, primary immune cells, their interaction with cell membranes and uptake, and the cytotoxic effects of biodegradation products.

2.7. Cytotoxic effects of MoS_2 and *f*-MoS_2

We have initially discussed the unprecedented advantages and superior performances of MoS_2 in the biomedical field [3]. Nevertheless, recent rapid advances in the use of new 2D nanomaterials for such purpose have raised important questions about their safety, similarly to the earlier case of carbon nanotubes and graphene.[3, 10] In order to identify new research directions, a critical evaluation of the possible toxicity of MoS_2 and its functionalized derivatives is needed. *In vitro* testing is the first crucial step in the road towards the approval of any new drugs or (bio)materials in the medical field.[18, 37]

For these reasons we tried to unravel the possible cytotoxicity of MoS_2 and *f*-MoS_2 using two different cell lines and primary immune cells. We used HeLa cells as both non-phagocytic epithelial and cancer cell model and RAW 264.7 macrophages as immune and phagocytic model. Concerning primary immune cells, hMDMs were obtained by differentiating monocytes from healthy donors. These types of primary cells were used to address the effects of MoS_2 and *f*-MoS_2 towards human immune cells. We carried out cell viability tests and evaluated primary cell activation and cytokine release as key cytotoxicity parameters.

The different cell types were exposed to increasing concentrations of MoS_2 or *f*-MoS_2 for 24 h. At the end of the incubation, the cell viability was determined by flow cytometry. Our data revealed that the viability of HeLa cells was not affected by both MoS_2 samples, even at the highest concentration used, corresponding to 100 μg mL^{-1} (**Figure 8A**). Concerning RAW 264.7 macrophages, the viability was reduced of about 20 % respect to the control, but only at high concentrations and only in the case of *f*-MoS_2 (**Figure 8B**). Viability was not affected when the same cells were exposed to the pristine material. A similar behavior was observed

for hMDMs as their healthy state was preserved within the entire concentration range of the two MoS_2 samples even when prolonging the exposure to MoS_2 and *f*-MoS_2 up to seven days (**Figure S14**).

Then we evaluated the impact of the two nanomaterials on the activation state of the immune cells. For this purpose, RAW 264.7 cells and hMDMs were exposed again to MoS_2 or *f*-MoS_2 for 24 h. After the incubation, the levels of expression of CD86, an important surface activation marker of antigen-presenting cells, were determined. Overall, the outcome of cell activation experiments on immune cells was consistent with cell viability results as no variation of CD86 levels in both RAW 264.7 cells and hMDMs was registered (**Figure 9A** and **9B**). To further investigate a potential pro-inflammatory effect of our two MoS_2 samples, the secretion of two key pro-inflammatory cytokines (i.e. TNFα and IL6) by RAW 264.7 macrophages and hMDMs was analyzed. No significant amounts of cytokines were detected in RAW 264.7 cell supernatants (data not shown). Similarly, the quantity of TNFα secreted by hMDMs was comparable to basal levels (**Figure S15**). Only at the highest concentration of pristine MoS_2 (100 μg mL^{-1}) we measured an increase of IL6 release although not significant. The result of our first series of experiments on different types of cells suggests an encouraging overall absence of acute toxicity and pro-inflammatory activating effect of MoS_2 or *f*-MoS_2, up to a concentration of 50 μg mL^{-1}.

2.8. Cytotoxicity of MoS_2 and *f*-MoS_2 degradation products

We have shown how MoS_2 and *f*-MoS_2 can be degraded *in test tube* by naturally present enzymes and peroxides. In particular, a rather fast degradation with low concentration of H_2O_2 (i.e. 50 μM) may occur, due to the natural overproduction of H_2O_2 by peroxidases.[21-22] Based on our degradation results *in test tube* (**Figure 3**, **Figures S5** and **S6)**, we would expect that MoS_2 samples are likely degraded also *in vivo* by phagocytic and cancer cells. Reticuloendothelial system degradation by resident macrophages and tumor degradation might both contribute to the renal clearance and body elimination of MoS_2 thus reducing its

accumulation in non-targeted organs and consequent cytotoxicity.[47] However, MoS_2 degradation products might exhibit cellular toxicity themselves, affecting, for example, clearance profile. As such possibility should not be ruled out, we decided to investigate the impact of the biodegradation products.

We started addressing this issue by performing cell viability and pro-inflammatory activation assays in cells exposed to MoS_2 and *f*-MoS_2 degradation products (named: MoS_2-DP and *f*-MoS_2-DP). Previous to cell exposure, the two material samples were treated (degraded) with 50 µM H_2O_2 for 14 (MoS_2-DP14 and *f*-MoS_2-DP14) or 30 days (*f*-MoS_2-DP30) (**Figure S7**). As already mentioned in the previous paragraphs, H_2O_2 concentration was chosen in order to mimic the intracellular concentration of the peroxide reported in the literature for leucocytes and cancer cells.[24, 26] Cells were exposed for 24 h to MoS_2-DP14, *f*-MoS_2-DP14 or *f*-MoS_2-DP30 and subsequently analyzed by flow cytometry.

The outcome of cell viability experiments was similar for HeLa and RAW 264.7 cells. We observed a significant reduction of viable cells when they were exposed to concentrations equal to or greater than 50 µg mL^{-1} (HeLa) or 25 µg mL^{-1} (RAW 264.3) of pristine MoS_2-DP14 (**Figure 10A** and **10B**). When the sample is functionalized (*f*-MoS_2-DP14), this effect is reduced in both cell lines (**Figure 10A** and **10B**). However, when the functionalized compound is degraded for 30 days (*f*-MoS_2-DP30), toxicity starts to appear (**Figure 10A** and **10B**), and it is more evident in the case of the macrophage cell line (a significant viability reduction is observed from 50 µg mL^{-1} of *f*-MoS_2-DP30).

These data suggest that the degradation products generated by pristine MoS_2 are cytotoxic at high concentrations. On the other hand, we have shown how, in cell-free degradation studies, *f*-MoS_2 was much more resistant to degradation by H_2O_2 compared to the pristine MoS_2 (**Figure 3** and **S7**). We can conclude that functionalization stabilizes MoS_2, slowing down its degradation and attenuating the toxic effects of the degradation products.

Despite the adverse effect on cell viability, MoS_2-DPs and *f*-MoS_2-DPs did not trigger any pro-inflammatory response in macrophages. In fact, the expression of CD86 on the surface of RAW 264.7 cells did not increase after incubation with both degraded compounds (**Figur**e **10C**). Consistently, no pro-inflammatory cytokines were detected in the cell supernatants (data not shown). These data, apparently inconsistent with cell viability results, might be explained by the quick death of highly activated macrophages. As a consequence, CD86 could not be detected by flow cytometry and cytokines could not have been produced in time.

It is worth noting that the effects on viability are only due to the degradation products of MoS_2 and not to the presence of H_2O_2. In fact, by treating the cells with buffer solutions prepared in order to mimic the H_2O_2 concentration in the samples used for the experiments, cell viability was not impaired (**Figure S16**).

2.9. Cellular interaction and internalization

Finally, to prove that the impact on cell viability and activation was due to the interaction and internalization of pristine and functionalized MoS_2 by the different cells, the uptake of these materials by HeLa cells and human monocyte-derived macrophages was investigated by TEM. For this purpose, the cells were exposed to 50 μg mL^{-1} of MoS_2 or *f*-MoS_2 for 24 h. The results showed a very efficient cell uptake of MoS_2 nanosheets, both pristine and functionalized, including the non-phagocytic HeLa cells. In **Figure 11A-D** (HeLa) and **11E** and **11F** (hMDMs), representative images of cells exposed to the MoS_2 samples for 24 h are shown. The materials were found both inside vesicles or free into the cytoplasm, behavior similar to graphene oxide [51]. This can be explained by the fact that MoS_2 and *f*-MoS_2 show a very high dispersibility in the aqueous media. In some cases, MoS_2 sheets penetrate the cell membrane as rolled needles (evidenced by a yellow arrow in **Figure S17**), similarly to carbon nanotubes and graphene oxide.[51-52]

Moreover, the formation of large invaginations of the cell membrane in correspondence to the materials indicates a probable internalization by ATP-dependent endocytic pathways (e.g.

macropinocytosis or phagocytosis in the case of hMDM).[51] The hypothesis is also reinforced by the intracellular MoS_2-containing vesicles. On the other hand, the free nanosheets in the cytoplasm can be the results of passive diffusion trough the plasma membrane or even endosome rupture.[51] There was not an evident difference in the mechanisms or entity of the cell uptake between the pristine and the functionalized material for both HeLa and hMDM cells. Additional studies on the elucidation of the precise cell uptake mechanisms are warrant, but beyond the scope of this work.

3. Conclusion

In summary, this is the first report on biodegradation of different types of highly water dispersible MoS_2 (pristine and functionalized) nanosheets by enzymatic catalysis of peroxidases (i.e. plant HRP and human MPO) in the presence of low concentration of H_2O_2. Interestingly, much quicker degradation compared to peroxidase treatment was observed in biologically relevant concentrations of H_2O_2 without any enzymes. Slow degradation was also evidenced in simple buffer solution. Our results confirm very recent reports showing *in vitro* and *in vivo* degradability and elimination of MoS_2 nanosheets. In addition, covalent functionalization of MoS_2 tunes the degradation profile, which becomes particularly interesting in the design of advanced biomedical tools (i.e. drug delivery carriers or implants). Overall, these *in vitro* degradation and cellular toxicity studies suggest an enhanced biocompatibility and a better biodegradability of MoS_2 nanosheets, promoting this material as a better candidate for biomedical applications compared to other carbon or 2D nanomaterials. Finally, assessing *in vivo* toxicity and biodegradation of pristine and functionalized MoS_2 nanosheets is the objective of our future research.

Supporting Information

Supporting Information is available from the Wiley Online Library or from the author. Experimental section with details on the materials and methods and additional characterizations

Acknowledgements

This work was supported by the Centre National de la Recherche Scientifique (CNRS), by the Agence Nationale de la Recherche (ANR) through the LabEx project Chemistry of Complex Systems (ANR-10-LABX-0026_CSC) and by the International Center for Frontier Research in Chemistry (icFRC). The authors gratefully acknowledge financial support from EU FP7-ICT-2013-FET-F GRAPHENE Flagship project (No. 604391). We wish to acknowledge Petra Hellwig and Frédéric Melin for giving access to Raman instrument, Cathy Royer and Valérie Demais for TEM analyses at the Plateforme Imagerie in Vitro at the Center of Neurochemistry (Strasbourg, France). We would like to thank Dris Ihiawakrim for HRTEM and SAED measurements.

References

[1] M. Chhowalla, H. S. Shin, G. Eda, L.-J. Li, K. P. Loh, H. Zhang, *Nat. Chem.* **2013**, 5, 263.
[2] P. Miró, M. Ghorbani-Asl, T. Heine, *Angew. Chem. Int. Ed.* **2014**, 53, 3015.
[3] R. Kurapati, K. Kostarelos, M. Prato, A. Bianco, *Adv. Mater.* **2016**, 28, 6052.
[4] J. Gao, B. Li, J. Tan, P. Chow, T.-M. Lu, N. Koratkar, *ACS Nano* **2016**, 10, 2628.
[5] Y. Rong, K. He, M. Pacios, A. W. Robertson, H. Bhaskaran, J. H. Warner, *ACS Nano* **2015**, 9, 3695.
[6] Q. Tang, D.-e. Jiang, *Chem. Mater.* **2015**, 27, 3743.
[7] D. Voiry, A. Goswami, R. Kappera, C. de Carvalho Castro e Silva, D. Kaplan, T. Fujita, M. Chen, T. Asefa, M. Chhowalla, *Nat. Chem.* **2015**, 7, 45.
[8] E. P. Nguyen, B. J. Carey, J. Z. Ou, J. van Embden, E. D. Gaspera, A. F. Chrimes, M. J. S. Spencer, S. Zhuiykov, K. Kalantar-zadeh, T. Daeneke, *Adv. Mater.* **2015**, 27, 6225.
[9] E. P. Nguyen, B. J. Carey, C. J. Harrison, P. Atkin, K. J. Berean, E. Della Gaspera, J. Z. Ou, R. B. Kaner, K. Kalantar-zadeh, T. Daeneke, *Nanoscale* **2016**, 8, 16276.
[10] D. Chimene, D. L. Alge, A. K. Gaharwar, *Adv. Mater.* **2015**, 27, 7261.
[11] Y. Chen, C. Tan, H. Zhang, L. Wang, *Chem. Soc. Rev.* **2015**, 44, 2681.
[12] Z. Chengzhou, D. Dan, L. Yuehe, *2D Materials* **2015**, 2, 032004.
[13] E. L. K. Chng, Z. Sofer, M. Pumera, *Nanoscale* **2014**, 6, 14412.

[14] K. Kalantar-zadeh, J. Z. Ou, T. Daeneke, M. S. Strano, M. Pumera, S. L. Gras, *Adv. Funct. Mater.* **2015**, 25, 5086.
[15] X. Wang, N. D. Mansukhani, L. M. Guiney, Z. Ji, C. H. Chang, M. Wang, Y.-P. Liao, T.-B. Song, B. Sun, R. Li, T. Xia, M. C. Hersam, A. E. Nel, *Small* **2015**, 11, 5079.
[16] W. Z. Teo, E. L. K. Chng, Z. Sofer, M. Pumera, *Chem. Eur. J.* **2014**, 20, 9627.
[17] E. L. K. Chng, M. Pumera, *RSC Adv.* **2015**, 5, 3074.
[18] K. Kostarelos, K. S. Novoselov, *Science* **2014**, 344, 261.
[19] L. Dong, S. Lin, L. Yang, J. Zhang, C. Yang, D. Yang, H. Lu, *Chem. Commun.* **2014**, 50, 15936.
[20] D. Trachootham, J. Alexandre, P. Huang, *Nat. Rev. Drug Discov.* **2009**, 8, 579.
[21] H. Pelicano, D. Carney, P. Huang, *Drug Resist. Updat.* **2004**, 7, 97.
[22] Y.-T. Chiang, Y.-W. Yen, C.-L. Lo, *Biomaterials* **2015**, 61, 150.
[23] M. Giorgio, M. Trinei, E. Migliaccio, P. G. Pelicci, *Nat. Rev. Mol. Cell Biol.* **2007**, 8, 722.
[24] C. de Gracia Lux, S. Joshi-Barr, T. Nguyen, E. Mahmoud, E. Schopf, N. Fomina, A. Almutairi, *J. Am. Chem. Soc.* **2012**, 134, 15758.
[25] H.-L. Pu, W.-L. Chiang, B. Maiti, Z.-X. Liao, Y.-C. Ho, M. S. Shim, E.-Y. Chuang, Y. Xia, H.-W. Sung, *ACS Nano* **2014**, 8, 1213.
[26] K. E. Broaders, S. Grandhe, J. M. J. Fréchet, *J. Am. Chem. Soc.* **2011**, 133, 756.
[27] V. Kagan, N. Konduru, W. Feng, B. Allen, J. Conroy, Y. Volkov, I. Vlasova, N. Belikova, N. Yanamala, A. Kapralov, Y. Tyurina, J. Shi, E. Kisin, A. Murray, J. Franks, D. Stolz, P. Gou, J. Klein-Seetharaman, B. Fadeel, A. Star, A. Shvedova, *Nat. Nanotechnol.* **2010**, 5, 354
[28] R. Kurapati, J. Russier, M. A. Squillaci, E. Treossi, C. Ménard-Moyon, A. E. Del Rio-Castillo, E. Vazquez, P. Samorì, V. Palermo, A. Bianco, *Small* **2015**, 11, 3985.
[29] G. P. Kotchey, B. L. Allen, H. Vedala, N. Yanamala, A. A. Kapralov, Y. Y. Tyurina, J. Klein-Seetharaman, V. E. Kagan, A. Star, *ACS Nano* **2011**, 5, 2098.
[30] A. R. Sureshbabu, R. Kurapati, J. Russier, C. Ménard-Moyon, I. Bartolini, M. Meneghetti, K. Kostarelos, A. Bianco, *Biomaterials* **2015**, 72, 20.
[31] C. Bussy, C. Hadad, M. Prato, A. Bianco, K. Kostarelos, *Nanoscale* **2016**, 8, 590.
[32] K. Bhattacharya, S. P. Mukherjee, A. Gallud, S. C. Burkert, S. Bistarelli, S. Bellucci, M. Bottini, A. Star, B. Fadeel, *Nanomed. Nanotechnol. Biol. Med.* **2016**, 12, 333.
[33] R. Kurapati, C. Backes, C. Ménard-Moyon, J. N. Coleman, A. Bianco, *Angew. Chem. Int. Ed.* **2016**, 55, 5506.
[34] B. L. Allen, P. D. Kichambare, P. Gou, I. I. Vlasova, A. A. Kapralov, N. Konduru, V. E. Kagan, A. Star, *Nano Lett.* **2008**, 8, 3899.
[35] B. L. Allen, G. P. Kotchey, Y. Chen, N. V. K. Yanamala, J. Klein-Seetharaman, V. E. Kagan, A. Star, *J. Am. Chem. Soc.* **2009**, 131, 17194.
[36] Y.-H. Fu, C.-Y. Chen, C.-T. Chen, *Polym. Chem.* **2015**, 6, 8132.
[37] Z. Wang, W. Zhu, Y. Qiu, X. Yi, A. von dem Bussche, A. Kane, H. Gao, K. Koski, R. Hurt, *Chem. Soc. Rev.* **2016**, 45, 1750.
[38] Z. Wang, A. von dem Bussche, y. qiu, T. M. Valentin, K. Gion, A. B. Kane, R. H. Hurt, *Environ. Sci. Technol.* **2016**, 50, 7208.
[39] M. Calandra, *Phys. Rev. B* **2013**, 88, 245428.
[40] K. S. Rabindar, G. B. Reddy, *J. Phys. D: Appl. Phys.* **2014**, 47, 065305.
[41] K. Routray, W. Zhou, C. J. Kiely, W. Grünert, I. E. Wachs, *J. Catal.* **2010**, 275, 84.
[42] M. M. Y. A. Alsaif, K. Latham, M. R. Field, D. D. Yao, N. V. Medehkar, G. A. Beane, R. B. Kaner, S. P. Russo, J. Z. Ou, K. Kalantar-zadeh, *Adv. Mater.* **2014**, 26, 3931.
[43] P. Chandra, D. S. Doke, S. B. Umbarkar, A. V. Biradar, *J. Mater. Chem. A* **2014**, 2, 19060.

[44] N. Kang, H. P. Paudel, M. N. Leuenberger, L. Tetard, S. I. Khondaker, *J. Phys. Chem. C* **2014**, 118, 21258.
[45] X. Shao, J. Tian, Q. Xue, C. Ma, *J. Mater. Chem.* **2003**, 13, 631.
[46] J.-M. Yun, Y.-J. Noh, C.-H. Lee, S.-I. Na, S. Lee, S. M. Jo, H.-I. Joh, D.-Y. Kim, *Small* **2014**, 10, 2319.
[47] J. Hao, G. Song, T. Liu, X. Yi, K. Yang, L. Cheng, Z. Liu, *Adv. Sci.* **2016**, DOI:10.1002/advs.201600160.
[48] T. K. M. C. K. Gupta, *Hydrometallurgy in Extraction Processes*, Vol. 2, CRC Press, 1990.
[49] M. Kan, J. Y. Wang, X. W. Li, S. H. Zhang, Y. W. Li, Y. Kawazoe, Q. Sun, P. Jena, *J. Phys. Chem. C* **2014**, 118, 1515.
[50] I. I. Vlasova, A. A. Kapralov, Z. P. Michael, S. C. Burkert, M. R. Shurin, A. Star, A. A. Shvedova, V. E. Kagan, *Toxicol. Appl. Pharmacol.* **2016**, 299, 58.
[51] J. Russier, E. Treossi, A. Scarsi, F. Perrozzi, H. Dumortier, L. Ottaviano, M. Meneghetti, V. Palermo, A. Bianco, *Nanoscale* **2013**, 5, 11234.
[52] L. Lacerda, J. Russier, G. Pastorin, M. A. Herrero, E. Venturelli, H. Dumortier, K. T. Al-Jamal, M. Prato, K. Kostarelos, A. Bianco, *Biomaterials* **2012**, 33, 3334.

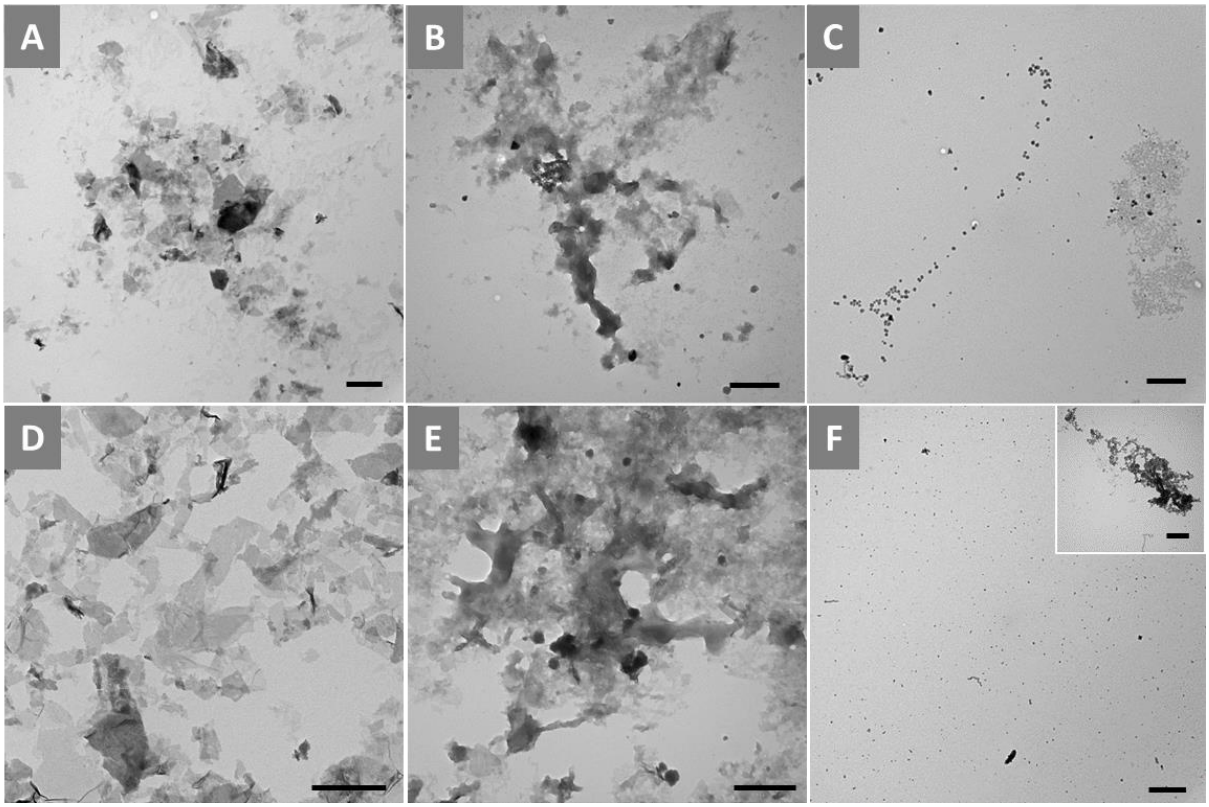

Figure 1. TEM images. Panel (A) shows MoS_2 sheets dispersed in water; (B) 20 day-treated MoS_2 sheets with HRP+H_2O_2; (C) 20 day-treated MoS_2 sheets only by addition of H_2O_2; panel (D) shows *f*-MoS_2 sheets dispersed in water; (E) 20 day-treated *f*-MoS_2 sheets with HRP+H_2O_2; and (F) 20 day-treated *f*-MoS_2 sheets only by addition of H_2O_2. Inset in (F) shows partially degraded nanosheets. Scale bars represent 500 nm in all images.

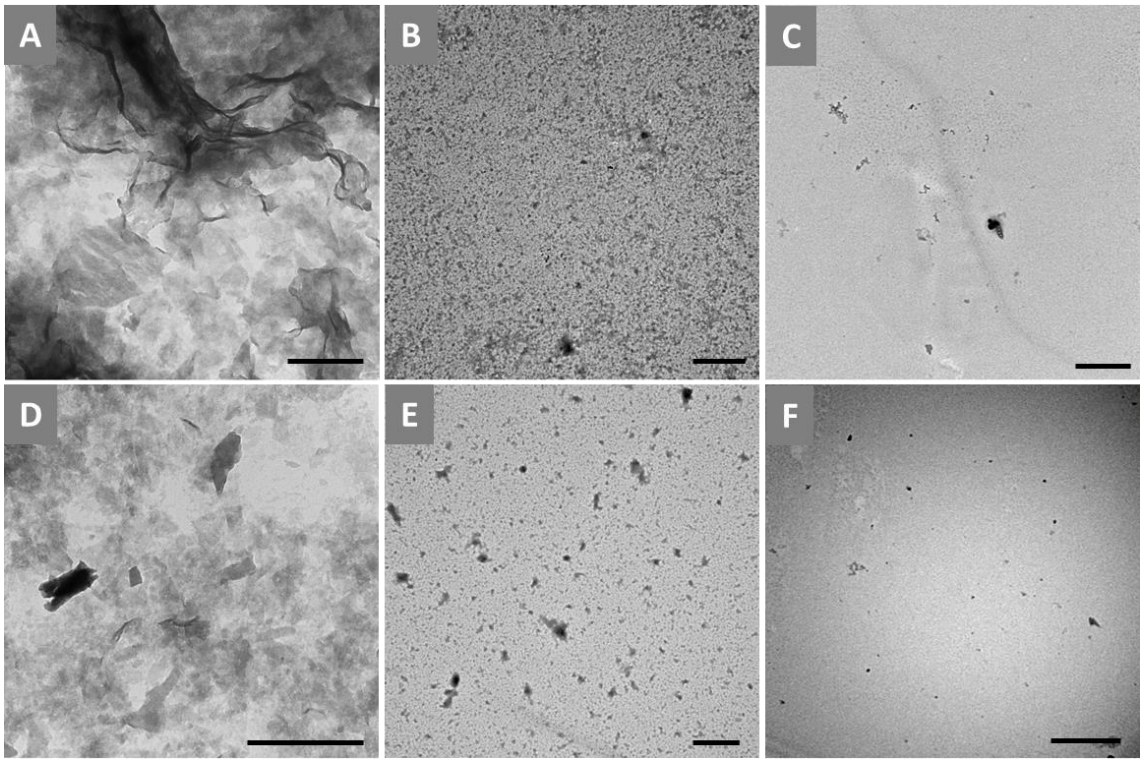

Figure 2. TEM images. Panel (A) shows MoS_2 sheets dispersed in PBS after 24 h; (B) 24 h treated MoS_2 sheets with MPO/NaCl/H_2O_2; (C) 15 h treated MoS_2 sheets by addition of only H_2O_2; panel (D) shows *f*-MoS_2 sheets dispersed in PBS after 24 h; (E) 24 h treated *f*-MoS_2 sheets with MPO/NaCl/H_2O_2; and (F) 20 h treated *f*-MoS_2 sheets by addition of only H_2O_2. Scale bars represent 500 nm in all images.

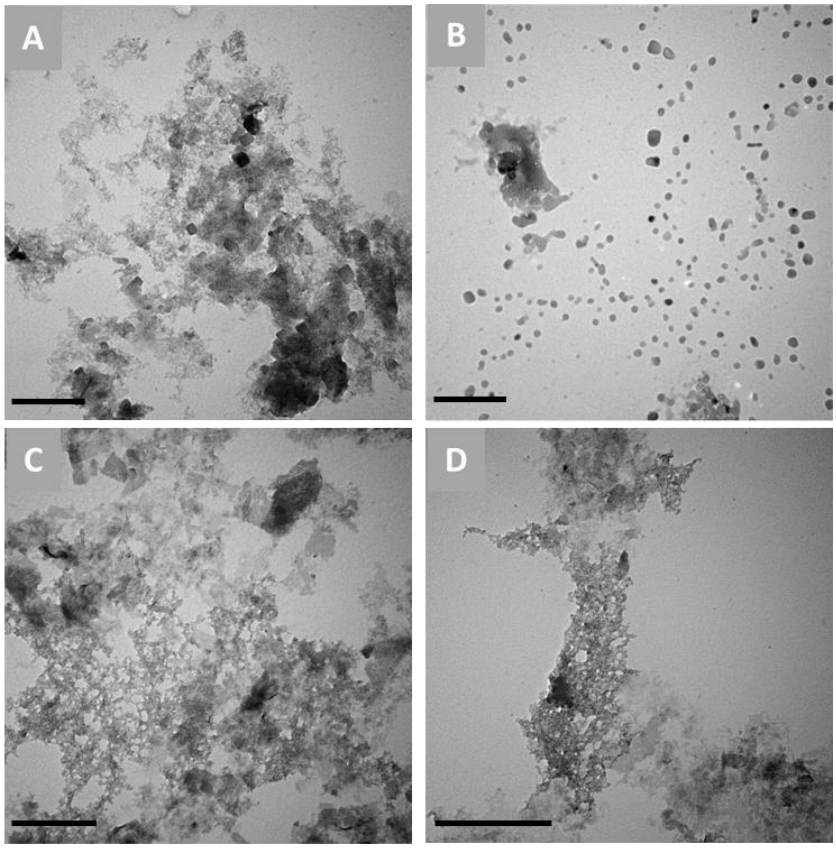

Figure 3. Panels (A) and (B) represent MoS_2 sheets after treating with 50 µM of H_2O_2 for 14 days; panels (C) and (D) represent *f*-MoS_2 sheets after treating with 50 µM of H_2O_2 for 14 and 30 days, respectively. Scale bars correspond to 500 nm.

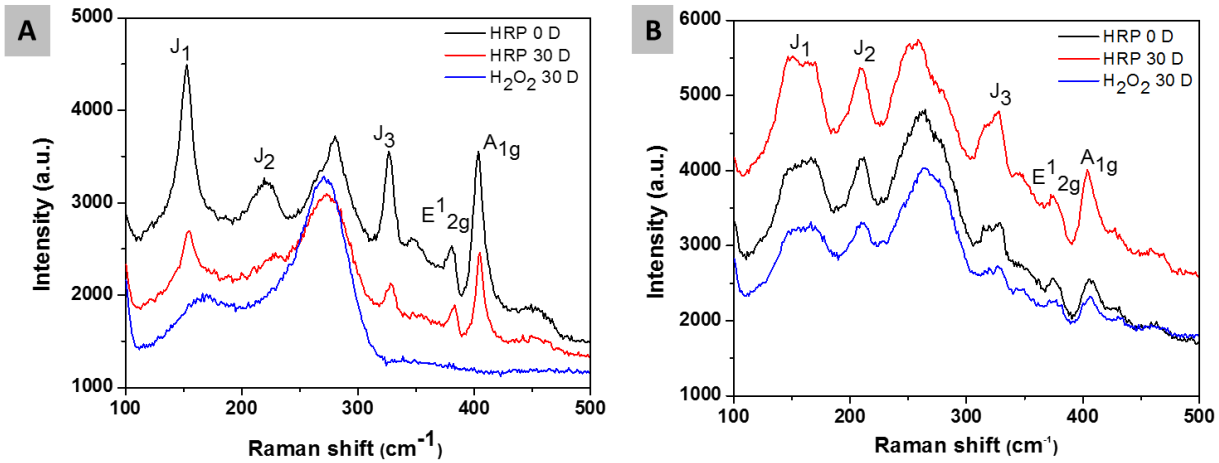

Figure 4. Raman analyses of HRP treated MoS_2 (A) and *f*-MoS_2 (B) sheets, respectively.

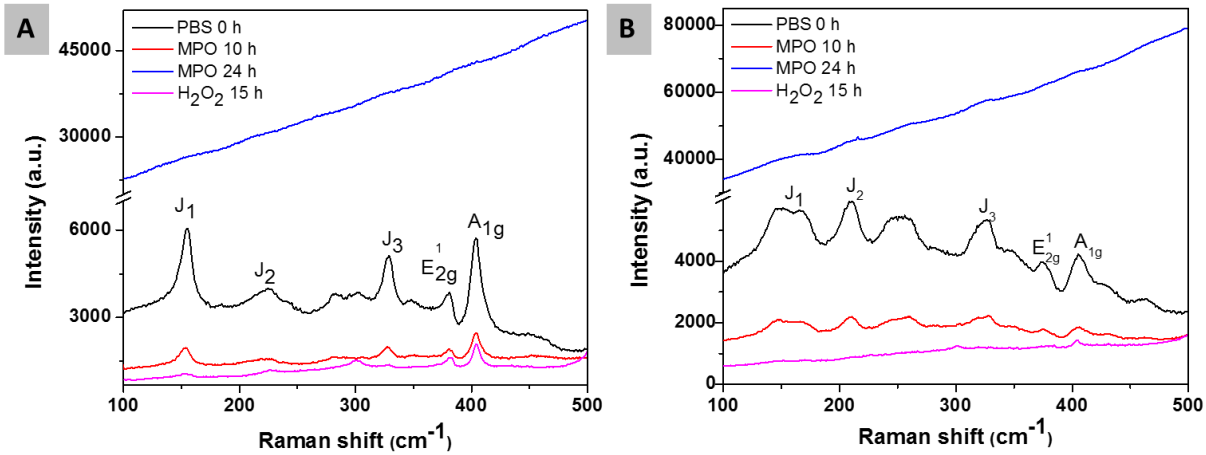

Figure 5. Raman analyses of MPO treated MoS_2 (A) and *f*-MoS_2 (B) sheets, respectively.

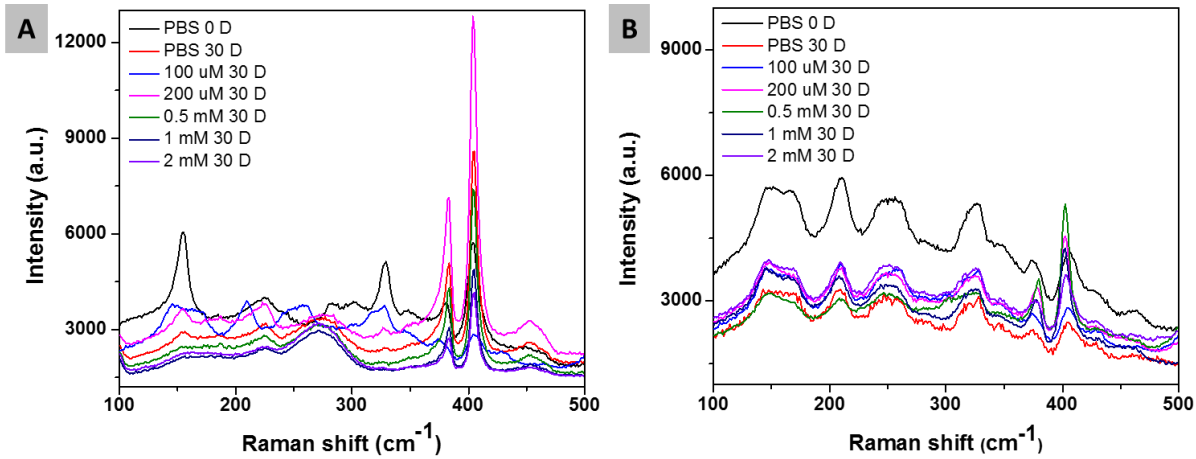

Figure 6. Raman analyses of MoS_2 (A) and *f*-MoS_2 (B) samples treated with different concentration of hydrogen peroxide, respectively.

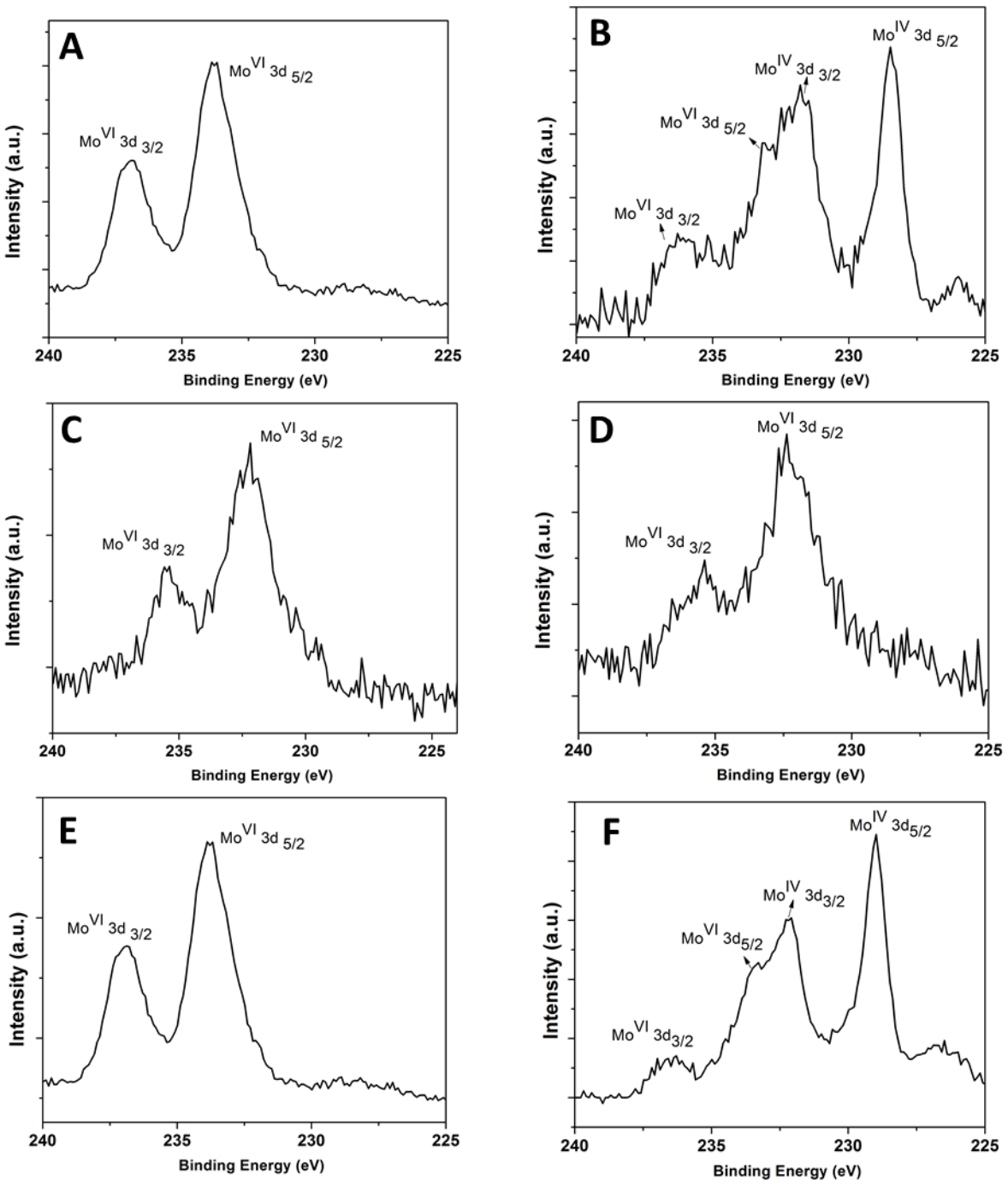

Figure 7. XPS analyses showing high-resolution spectra of Mo 3d binding energy of MoS_2 and *f*-MoS_2 treated with HRP+H_2O_2 (after 30 d; A & B), MPO+H_2O_2 (after 20 h; C & D), H_2O_2 alone (after 14 for MoS_2 and 30 d for *f*-MoS_2; E & F).

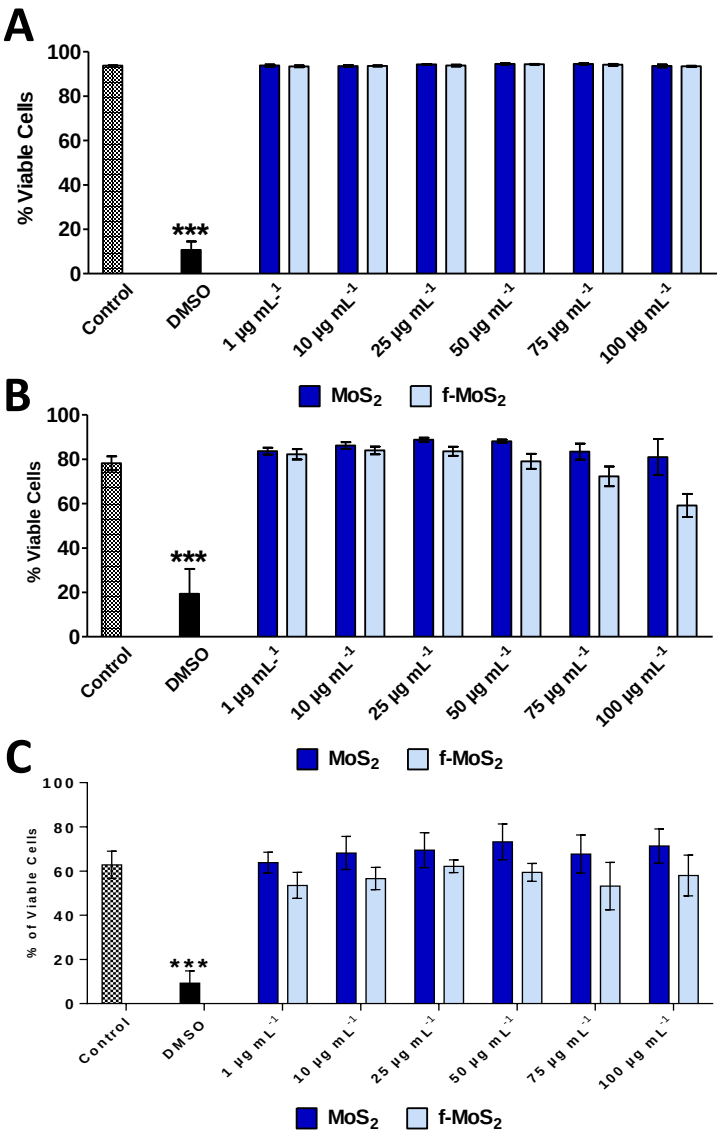

Figure 8. Flow cytometry analysis of HeLa (A), RAW 264.7 (B) and hMDM (C) cell viability exposed to different concentrations of MoS_2 or *f*-MoS_2 for 24 h. Two-ways ANOVA followed by Bonferroni's post-test was performed to determine the statistical differences versus control cells and to compare MoS_2 and *f*-MoS_2 samples to each other (*$p<0.05$; **$p<0.01$; ***$p<0.001$).

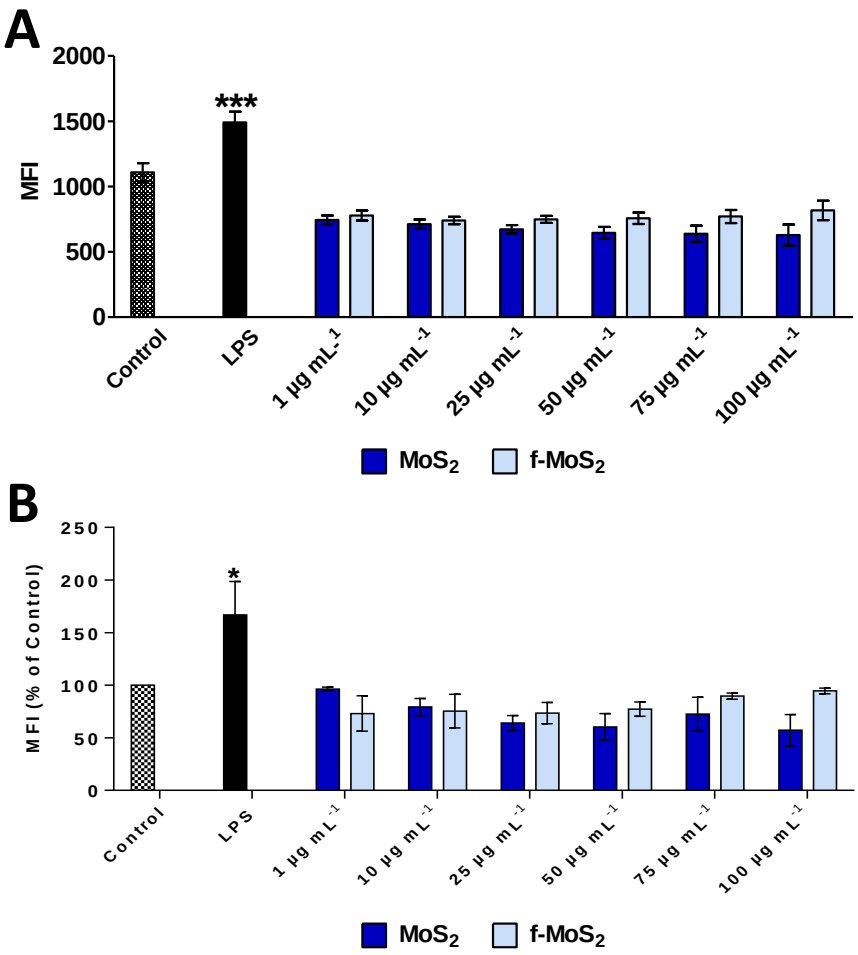

Figure 9. Flow cytometry analysis of CD86 surface expression in RAW 264.7 cells (A) and hMDMs (B) after exposure to different concentrations of MoS_2 or *f*-MoS_2 for 24 h. Two-ways ANOVA followed by Bonferroni's post-test was performed to determine the statistical differences versus control cells and to compare MoS_2 and *f*-MoS_2 samples to each other (*p<0.05; **p<0.01; ***p<0.001).

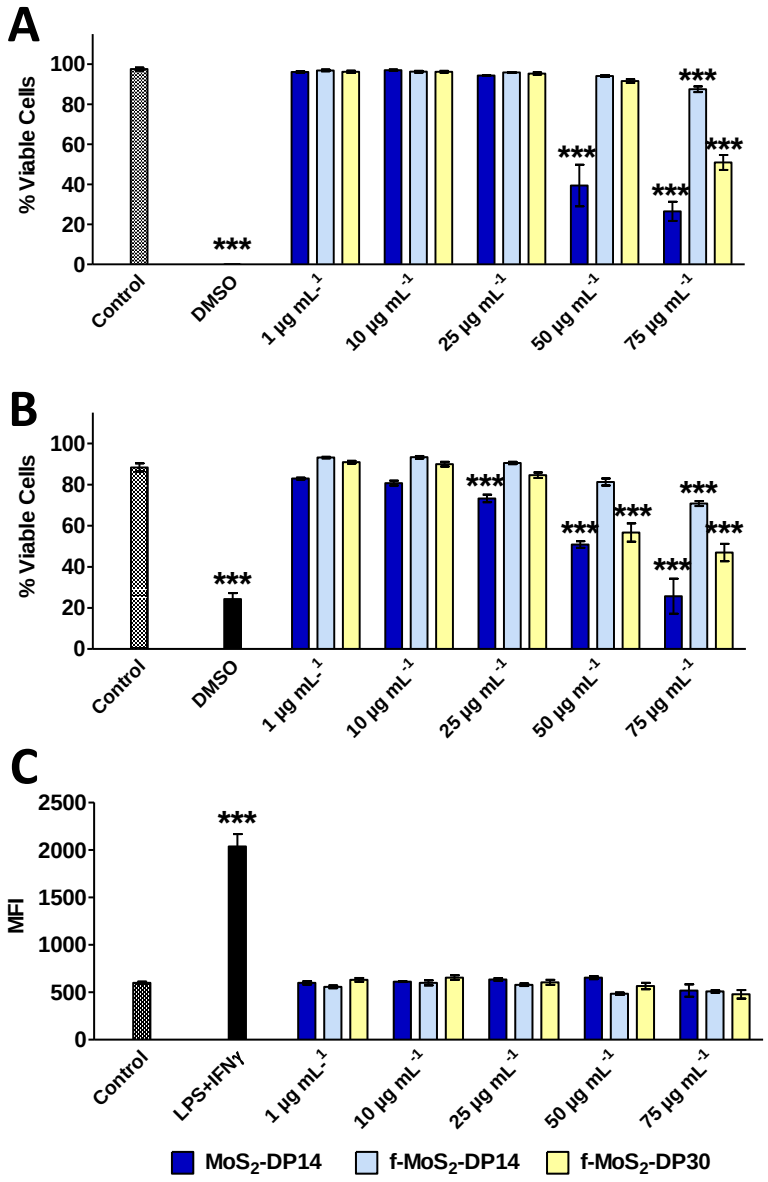

Figure 10. Flow cytometry analysis of cell viability in HeLa (A), RAW264.7 (B) cells exposed to different concentrations of degraded MoS_2 or *f*-MoS_2 for 24 h. Flow cytometry analysis of the cell activation marker CD86 in RAW 264.7 cells (C) after exposure to different concentrations of degraded MoS_2 or *f*-MoS_2 for 24 h. Two-ways ANOVA followed by Bonferroni's post-test was performed to determine the statistical differences versus control cells (*$p<0.05$; **$p<0.01$; ***$p<0.001$).

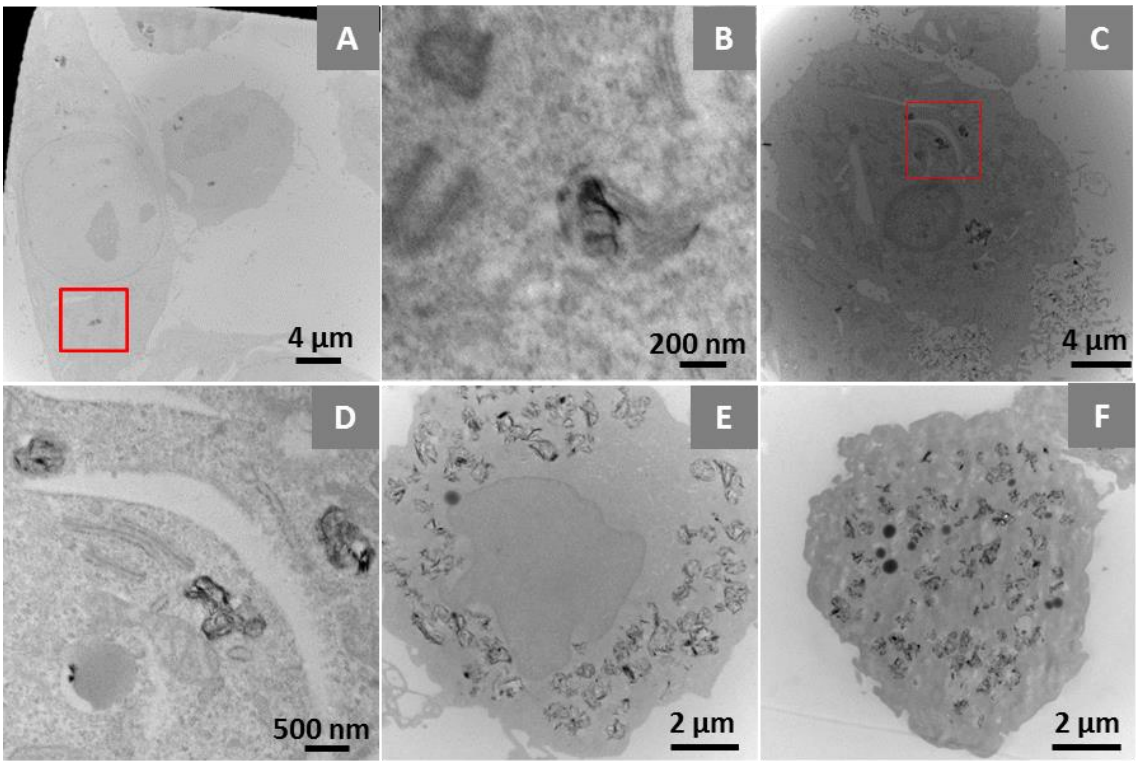

Figure 11. TEM images of HeLa cells (A-D) and hMDMs (E-F) incubated with MoS_2 or *f*-MoS_2 (50 µg mL^{-1}). HeLa cells incubated with MoS_2 (A-B) and *f*-MoS_2 (C-D) for 24 h, respectively. hMDMs incubated with MoS_2 (E) and *f*-MoS_2 (F) for 24 h, respectively. The red squares in the images are enlarged in the respective closed right panels.

Supporting Information

Experimental Section

1. Materials

Hyman MPO (hMPO) derived from human neutrophils (Athens Research and Technology, USA) has an activity of 180-220 U mg^{-1}. Diethylenetriamine pentaacetic acid (DTPA), hydrogen peroxide (30% aqueous solution), NaCl, $NaH_2PO_4 \cdot 2H_2O$ and $Na_2HPO_4 \cdot 2H_2O$ were purchased from Alfa Aesar and used directly without any further purification. Horseradish peroxidase (HRP) type VI-salt free powder (activity = 250-330 U mg^{-1}) was obtained from Sigma-Aldrich. Phosphate buffered saline (PBS) without Ca^{2+} or Mg^{2+} ions was purchased from Lonza. Deionized water was obtained using a Millipore filter system MilliQ®.

2. Synthesis of MoS_2 and functionalized MoS_2

Pristine MoS_2 nanosheets and functionalized MoS_2 (*f*-MoS_2) with acetamide groups were synthesized and characterized according to a previous work.[1] Briefly single-layer MoS_2 were obtained via chemical intercalation with lithium. MoS_2 powder (0.3g, Sigma) was dispersed in hexane under argon. n-Butyllithium (3 mL, Sigma; CAUTION: n-butyllithium is highly pyrophoric!) was then injected in the solution and the mixture was heated at reflux. After 48 h, the intercalated powder was recovered by filtration and washed with hexane (4×50mL). The intercalated powder was then dissolved in water at 1 mg/mL and sonicated for 1 h. The dispersed nanosheets were then washed 3 times with MilliQ water to completely remove lithium cations. Non-exfoliated materials were finally removed by low-speed centrifugation.

Functionalized MoS_2 was prepared from chemically exfoliated MoS_2. MoS_2 nanosheets dispersed in water were mixed with tenfold excess of 2-iodo acetamide (Sigma). After 5 days of reaction at room temperature, the solution was washed via centrifugation with 2-propanol (3×50 mL), ethanol (3×50 mL) and water (3×50mL).

MoS_2 and *f*-MoS_2 were characterized by Raman, X-ray photoelectron (XPS) spectroscopy, which confirmed the presence of 1T and 2H phase (Figure S1A-E). The presence of 1T phase in the functionalized MoS_2 was also observed by scanning transmission electron microscopy (STEM) (Figure 1F). By XPS, a peak at 400 eV as well as a shoulder at 288.4 eV demonstrate the presence of C-NH_2 and C=O functions, respectively, and are attributed to the amide group (Figure 1C, D). By careful examination of the S*2p* regions, we can identify the S-C bonds confirming the successful covalent functionalization of the MoS_2 nanosheets (Figure 1B). According to XPS, we estimated the amount of functional groups per MoS_2 to be ~ 30 %.

3. Raman Analyses

Raman analysis of all MoS_2 samples was performed using Raman spectra Renishaw inVia microRaman equipped with 514 nm laser and a Leica microscope. All spectra were recorded with 5% laser power using 50× objective lens. All samples for Raman analysis were prepared by drop-casting 10 µL of respective samples on a Si window (ThorLabs) and dried for 24 h at room temperature. For each sample, five (minimum) to ten spectra were collected at different points of the sample. The recorded spectra were manually baseline-corrected using OriginLab software and averaged for a given data set. The average spectra are displayed in the main manuscript.

4. Zeta potential measurements

MoS_2 samples were sonicated for 1 min before zeta potential measurements and all measurements were performed using Zetasizer Nano S (Malvern Instruments) spectrometer operating under 633 nm laser irradiation. The zeta potential measurements were carried out at pH 7.

5. Transmission electron microscopy

For TEM characterization, 6 µL of each suspension of MoS_2 samples were deposited on carbon coated copper grids and dried for 24 h before the analysis. All samples were analyzed by a Hitachi H7500 microscope (Tokyo, Japan) with an accelerating voltage of 80 kV, equipped with a AMT Hamamatsu camera (Tokyo, Japan). For HRTEM and SAED analyses were performed on a JEOL 2100F TEM/STEM electron microscope operating at 200 kV.

6. XPS analysis

After treatment with HRP, hMPO and H_2O_2, pristine MoS_2 and *f*-MoS_2 solutions were lyophilized, re-dispersed in the minimum amout of water, drop-casted onto freshly cleaned silicon wafers and dried overnight. XPS analysis was carried out using a Thermo Scientific K-ALPHA photoelectron spectrometer with a basic chamber pressure of 10^{-8}-10^{-9} bar and an Al anode as X-ray source (1486 eV). Spot size of 400 µm was used. The analysis was repeated three times for each sample. The survey spectra are an average of 10 scans taken with a pass energy of 200.00 eV and a step size of 1 eV. The high resolution spectra are an average of 10 scans taken with a pass energy of 50.00 eV and a step size of 0.1 eV. An electron gun was turned on during analysis. For data analysis a shirley background subtraction was performed and no charge correction was applied. The differences in the signal intensities of the XPS spectra (Figure 7 and Figure S13) of the three conditions (HRP, hMPO and H_2O_2) are due to the varied amounts of the final solutions recovered (see the volumes of the solutions used in the the degradation procedures describes below). In addtion, the presence of salts and enzymes in the buffer used for the treatments contributes to the low signal intensities.

7. Enzymatic degradation by HRP

For the pristine MoS_2, a stock suspension of 0.47 mL of aqueous MoS_2 was added to 1.53 mL of PBS (final concentration of MoS_2: 0.1 mg mL^{-1}), final volume was 2 mL. For *f*-MoS_2, a stock suspension of 1.34 mL of aqueous *f*-MoS_2 were added to 0.66 mL of PBS (*f*-MoS_2 final concentration: 0.1 mg mL^{-1}), final volume was 2 mL.

To both suspensions, 0.35 mg of HRP were added in each vial. To enable the enzymatic activity of HRP, 8 µL of 10 mM H_2O_2 were added once every day up to 30 days. All suspensions were kept in the dark at room temperature and stirred for the entire duration of the experiment. Aliquots (50 µL) were taken at time points 0, 10, 20 and 30 days and stored at -20 °C in the dark until characterization by different techniques. The control experiments without addition of HRP were also prepared in the same way with only 8.0 µL of 10 mM H_2O_2 added every day up to 30 days. Both the degradation experiemnts were repeated two times.

8. Enzymatic degradation of MoS_2 by hMPO

A stock suspenion of 120 µL of MoS_2 (420 µg mL^{-1}) was added to 330 µL of 50 mM phosphate buffer containing 140 mM NaCl and 100 µM DTPA (MoS_2 final concentration: 0.1 mg mL^{-1}). To this suspension, 50 µL of hMPO (1 µg $µL^{-1}$), pre-dissolved in 50 mM phosphate, buffer was added. Then, 200 µM concentration of H_2O_2 was added (5 µL of 10 mM of H_2O_2) every hour for 24 h in total. hMPO was renewed every 5 h (5 additions: at 0, 5, 10, 15 and 20). The reaction mixture was maintained at 37 °C in the incubator. Aliquots (25 µL) were taken at time points 0, 10, 15, 20 and 24 h, and stored at -20 °C in the dark room until their characterization by different techniques.

For the degradation with H_2O_2 in the absence of hMPO, 120 µL of MoS_2 (final concentration: 0.1 mg mL^{-1}) were added to 380 µL of 50 mM phosphate buffer containing 140 mM NaCl and 100 µM DTPA. Then, 200 µM concentration of H_2O_2 was added (5 µL of 10 mM of H_2O_2) every hour for 24 h in total. Similarly, degradation of *f*-MoS_2 was also carried out, where 333 µL of *f*-MoS_2 aqeuous stock suspension (150 µg mL^{-1}) was added to 117 µL of 50 mM phosphate buffer containing 140 mM NaCl and 100 µM DTPA (final concentration: 0.1 mg/mL. To this suspension, 50 µL of hMPO (1 µg $µL^{-1}$) pre-dissolved in 50 mM phosphate buffer was added. For the degradation with only H_2O_2, 333 µL of *f*-MoS_2 (final concentration: 0.1 mg mL^{-1}) were added to 380 µL of 50 mM phosphate buffer containing 140 mM NaCl and 100 µM DTPA. Then, 200 µM concentration of H_2O_2 was added (5 µL of 10 mM of H_2O_2) every hour for 24 h in total. Both the degradation experiemnts were repeated two times.

9. Degradation by H_2O_2

0.24 mL of MoS_2 aqueous suspension having 420 µg mL^{-1} concentration were added to 0.73 mL of phosphate buffer saline (MoS_2 final concentration: 0.1 mg mL^{-1}).

0.66 mL of *f*-MoS_2 aqueous stock suspension having 150 µg mL^{-1} concentration was added to 0.34 mL of phosphate buffer saline (final concentration: 0.1 mg/mL).

Totally 7 vials for both MoS_2 were prepared. H_2O_2 concentration was varied as 0, 10, 100, 200, 500 µM, 1 mM and 2 mM. All sample vials were kept at 37 °C in the incubator up to 30 days.

We observed the color change of MoS_2 and *f*-MoS_2 and took aliquots at fixed intervals for Raman and TEM analyses. For each fixed intervals, digital photos were taken after sonicating for 1 or 2 minutes to get the better dispersed images to visualize the suspensions clearly.

10. Materials preparation for biological experiments

MoS_2 or *f*-MoS_2 stock solutions in water (420 µg mL^{-1} or 150 µg mL^{-1}, respectively) were diluted to new stock solutions in complete medium (336 µg mL^{-1} or 120 µg mL^{-1}, respectively) according to the following protocol: 1920 µL of either MoS_2 or *f*-MoS_2 + 240 µL RPMI (10X) + 240 µL FBS. The so-obtained new stock solutions were diluted in normal complete RPMI medium at the final concentrations used for the cell treatment.

11. Material degradation for biological experiments

0.48 mL of MoS_2 aqueous stock solution was added to 1.52 mL of PBS (final concentration: 0.1 mg mL^{-1}). To this suspension, 10 µL of 10 mM H_2O_2 were added to get 50 µM as final H_2O_2 concentration. Similarly, the controlled samples was prepared without adding H_2O_2.

1.32 mL of *f*-MoS_2 aqueous stock solution was added to 0.68 mL of PBS (final concentration: 0.1 mg mL^{-1}). To this, 10 µL of 10 mM H_2O_2 were added to get 50 µM as final H_2O_2 concentration. Similarly, the controlled sample was prepared without adding H_2O_2.

All the samples vials were maintained at 37 °C in the incubator for 14 days for MoS_2 sample and 14 and 30 days for *f*-MoS_2 respectively

Degraded MoS_2 samples were then used to prepare an 80 µg $µL^{-1}$ stock solution in all cases. Briefly, 1920 µL of either MoS_2-DP14, *f*-MoS_2-DP14 or 30 *f*-MoS_2-DP30 were mixed with 240 µL RPMI (10X) and 240 µL FBS in order to obtain suitable culture conditions. Afterwards, the stock solution was diluted accordingly with RPMI to obtain the working concentrations.

12. Buffer preparation for the H_2O_2 toxicity test

For the toxicity test two different concentrations of H_2O_2 were tested, 50 mM and 100 mM. In each of the cases, a stock solution was first prepared by adding 1000 µL of H_2O_2 + 125 µL

RPMI (10X) and 125 µL FBS. The stock solution was subsequently diluted with RPMI (1X) to simulate the working concentrations of MoS_2 or *f*-MoS_2 as it follows:

1 µg/ml: 4.4 µL stock solution + 345.6 RPMI (1X)

10 µg/ml: 44 µL stock solution + 306 RPMI (1X)

20 µg/ml: 87.5 µL stock solution + 2625 RPMI (1X)

40 µg/ml: 175 µL stock solution + 175 RPMI (1X)

80 µg/ml: 350 µL stock solution + 0 RPMI (1X)

13. Human monocyte derived macrophages (hMDM). Leukocyte-rich buffy coats from healthy adult donors were obtained from the French Blood Bank (Etablissement Français du Sang, Strasbourg, FRANCE) and peripheral blood mononuclear cells (PBMCs) were collected by Ficoll-Histopaque-1077 (Sigma) density gradient centrifugation.[2-4]

$CD14^+$ monocytes were then separated from PBMCs by immunomagnetic positive selection using an anti-CD14 monoclonal antibody coupled to magnetic beads followed by MACS column separation (Miltenyi Biotech), according to the manufacturer's protocol. The purity of isolated monocytes was assessed by flow cytometry using FITC-Mouse anti-Human CD14 antibodies (Clone M5E2, BD Pharmingen 555397) and hMDM were obtained by culturing them in complete RPMI 1640 medium (i.e. containing 10% heat inactivated FBS, 10 µg/ml gentamycin, and 10 mM HEPES; Lonza) supplemented with 12.5 ng/ml macrophage colony stimulating factor (M-CSF; ImmunoTools) in 12 well plates at a density of $3 \cdot 10^6$ cells/well for 7 days (37 °C, 5 % CO_2).[5-6] After differentiation, hMDM were detached with SE buffer (PBS containing 2 mM EDTA and 2% FBS), counted, reseeded in 96 well plates at a density of 2-$3 \cdot 10^5$ cells/well and allowed to adhere 4 h (37 °C, 5% CO_2) prior to MoS_2 exposure. Medium was then removed and cells incubated with MoS_2 and *f*-MoS_2 (1, 10, 25, 50, 75 and 100 µg/ml) during 24 h to 7 days.

14. Flow cytometry

Cellular viability. For cell viability/activation experiments, HeLa and RAW 264.7 cells were seeded into 96-well plates at a density of 10^5 cells/well and allowed to adhere overnight. The cells were then exposed to different concentrations of MoS_2, *f*-MoS_2, MoS_2-DP or *f*-MoS_2-DP, for 24 h. The cytotoxicity of MoS_2 and *f*-MoS_2 towards human macrophages (hMDMs) was evaluated by flow cytometry. For this purpose, cells were exposed to 1, 10, 25, 50, 75 and 100 µg/ml of our two MoS_2 samples. DMSO (20 %) was used as cellular death positive control. After incubation, cells were harvested with trypsin or SE buffer (hMDMs) and stained with both FITC-Annexin V (AnnV; BD Pharmingen 556419) and propidium iodide (PI, 0.2 µg mL^{-1}; Sigma-Aldrich) in a calcium containing buffer. The percentage of live (AnnV-/PI-) was

determined by acquiring at least 25000 events using a Gallios Flow Cytometer (Beckman Coulter) and analyzing the data with FlowJo software.

Cellular activation. Cellular activation of macrophages (RAW 264.7 and hMDMs) was evaluated by flow cytometry after incubation with MoS_2 and *f*-MoS_2 (1, 10, 25, 50, 75 and 100 µg/mL). Cellular activation was explored through CD86 expression evaluation. Briefly, after MoS2 treatment, human macrophages were detached with SE buffer and stained with FITC-Mouse anti-Human CD86 antibodies (Clone 2331(FUN-1), BD Pharmingen 555658), prior to flow cytometry acquisition. Lipopolysaccharide (LPS) alone (100 ng/ml for hMDM) or in combination with interferon γ (IFN γ, 1 ng mL^{-1} with LPS 1 µg mL^{-1} for RAW 264.7) was used as cell activation positive control. The CD86 associated fluorescence intensities were determined by acquiring at least 25,000 events using a Gallios Flow Cytometer (Beckman Coulter) and analyzing the data on $CD14^+$ hMDM or RAW 264.7 live cells gated populations with FlowJo software.

15. Pro-inflammatory cytokine determination. After exposure to MoS_2 and *f*-MoS_2 (1, 10, 25, 50, 75 and 100 µg/mL), cell supernatants were collected and the levels of inflammatory cytokines, including tumor necrosis factor alpha (TNFa), and interleukine-6 (IL6) were detected by ELISA. LPS alone (100 ng/mL for hMDMs) or in combination with interferon γ (IFN γ, 1 ng mL^{-1} with LPS 1 µg mL^{-1} for RAW 264.7) was used as pro-inflammatory cytokine production positive control. Secretion of human cytokines (hTNFα and hIL6) was measured using a double sandwich ELISA. Specific pairs of capture and biotinylated detection antibodies were used and respective recombinant TNFα and IL6 were taken as standards.

16. Transmission electron microscopy of HeLa and hMDMs. For TEM observation, HeLa cells or hMDMs were seeded into 24-well plates on glass coverslips at a density of $2 \cdot 10^5$ cells per well and allowed to adhere overnight. Cells were then exposed to 50 µg mL^{-1} of MoS_2 or *f*-MoS_2 for 24 hours for the cellular uptake studies. hMDMs were obtained as previously described but cultured on glass coverslips in 24-well plates at the density of $5\text{-}6 \cdot 10^5$ cells/well and allowed to adhere prior to MoS_2 exposure (50 µg mL^{-1}) during 24 h to 7 days.

At the end of incubation time, cells were washed with Tris buffer saline (TBS) and fixed overnight at 4 °C with 2.5% glutaraldehyde. On the following day, cells were washed twice in distilled water and then submitted to a secondary fixation with 1% aqueous osmium tetroxide (30 min at room temperature). After rinsing cells three times with distilled water, dehydratation was performed through a series of baths: twice with 50% ethanol (10 min), once with 70% ethanol (20 min), once with ethanol 95% (10 min), twice with absolute ethanol

(10 min) and finally twice with propylene oxide (for 10 min each). Infiltration with epoxy resin Epon was done using mixtures of propylene oxide and Epon resin in 2:1 (1 h) and 1:2 (1 h) ratio and finally with pure resin (1 h). On the last day, resin was replaced with fresh one and further incubated during 3 hours. Polymerized block with embedded cells were then prepared filling gelatine capsules with fresh resin and placing them upon the glass coverslips on which cells were grown. The as prepared capsules were then placed into the oven to polymerize the resin at 60 °C for 48 h afterwards glass coverslips were removed from the polimerized block surface and ultrathin sections (65-85 nm thick) were obtained using an ultramicrotome (Leica) with a diamond knife (DiATOME). The ultrathin sections were then collected on butvar-coated single-slot copper grids, stained with 1% uranyl acetate for 30 min and with lead citrate for 2 min. Grids were then examined by TEM (Hitachi H600). The ultrathin sections were then collected on 300-mesh copper grids and the images were carried out with a Hitachi H7500 instrument.

17. Statistical analyses

Data are presented ± SEM. Statistical analyses were performed using a two-way ANOVA test followed by Bonferroni's post-test. All p values < 0.05 were considered significant. The experiments shown for hMDMs are a summary of the data from at least three separate experiments run in triplicate, each based on cells from one human healthy donor. All data are presented ± SEM. Statistical analyses were performed using GraphPad software. Treatment effects were analyzed using two-way ANOVA followed by Bonferroni's post-test. All p values < 0.05 were considered significant.

18. Equations of MoS_2 oxidation

$$MoS_2 + 9\ H_2O_2 \rightarrow MoO_3 + 7\ H_2O + 2\ H_2SO_4 \quad (1)^{[7]}$$

$$MoS_2 + 9\ OCl^- + 6\ OH^- \rightarrow MoO_4^{2-} + 3\ H_2O + 2\ SO_4^{2-} + 9\ Cl^- \quad (2)^{[8]}$$

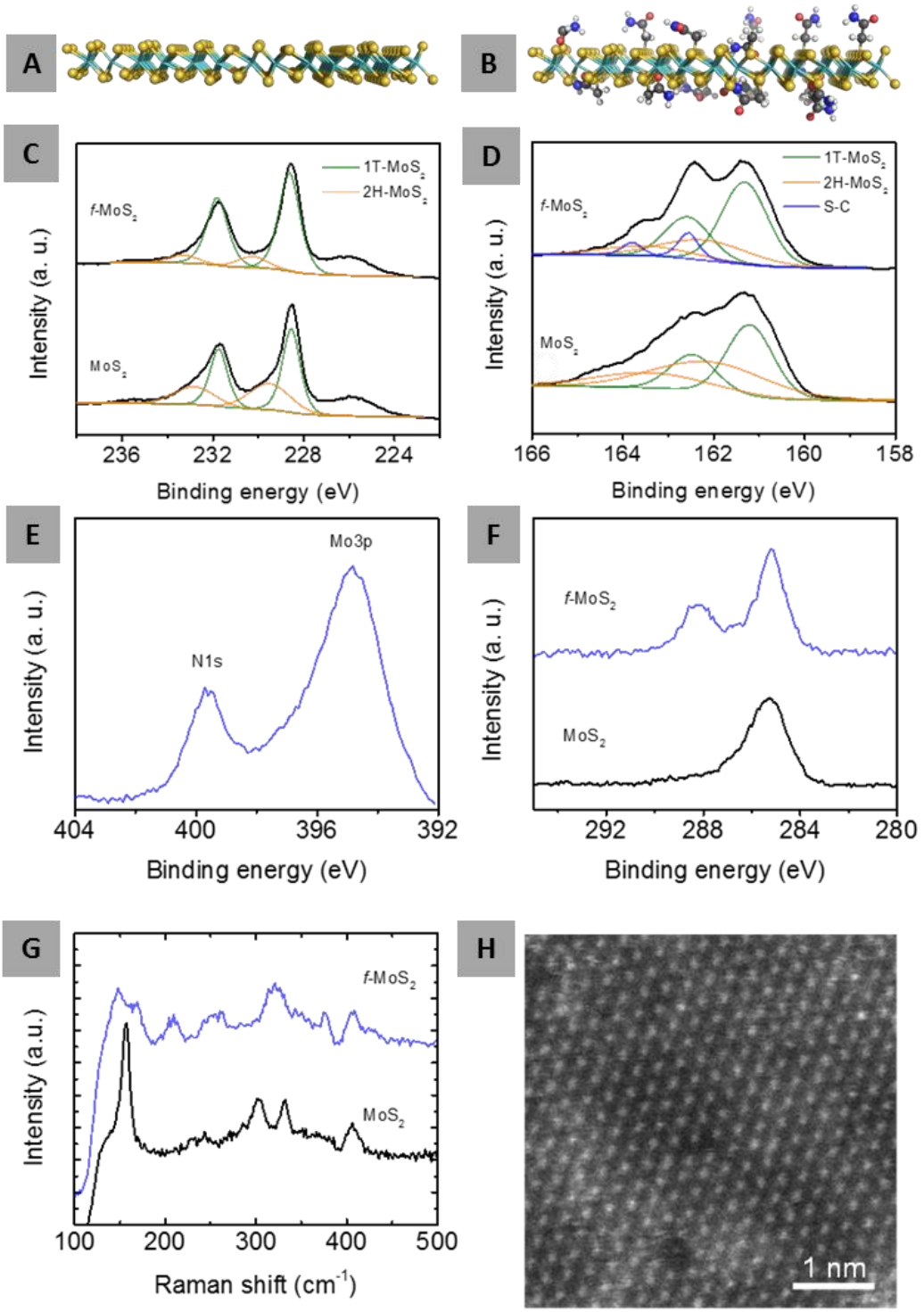

Figure S1: 1T phase structure of the pristine MoS_2 and covalently functionalized *f*-MoS_2 with acetamide groups are shown in (A) and (B), respectively. High resolution XPS spectra of as-exfoliated MoS_2 and functionalized MoS_2 from the Mo*3d* (C), S*2p* (D), N*1s* (E) and C*1s* (F) regions. Panels G and H present the Raman spectra of MoS_2 and *f*-MoS_2 and STEM image of *f*-MoS_2, respectively.

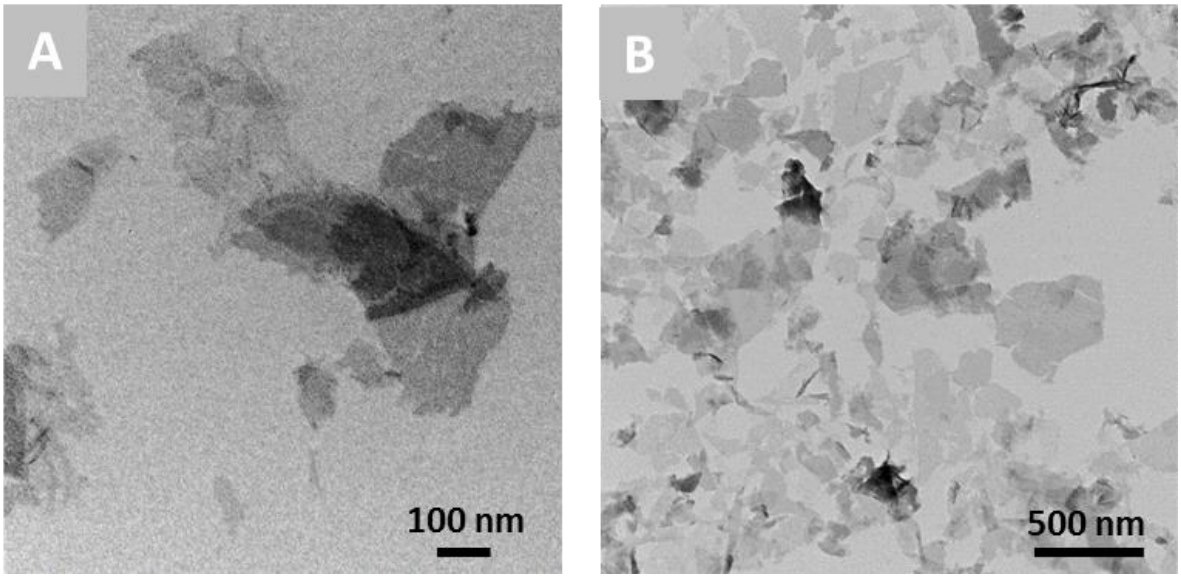

Figure S2: TEM images of MoS_2 and *f*-MoS_2 sheets dispersed in water.

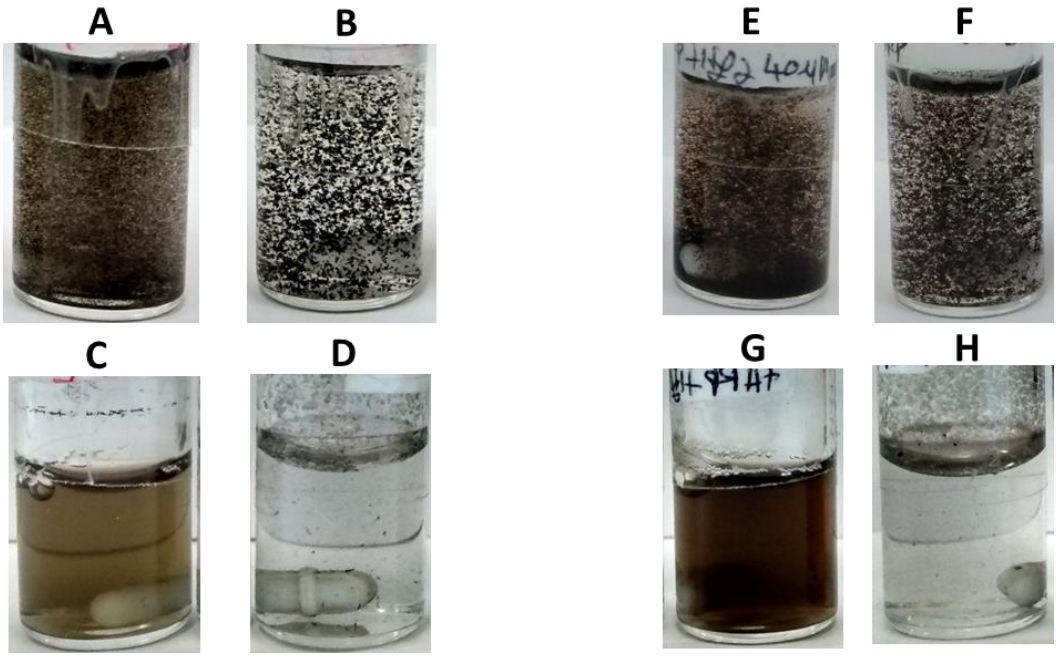

Figure S3: Images of MoS_2 and *f*-MoS_2 samples dispersed in PBS: Panels (A and B) represents the MoS_2 samples at 0 day treated with HRP + H_2O_2 and H_2O_2 alone, respectively; panels (C and D) represents MoS_2 samples at 20 day-treated with HRP + H_2O_2 and H_2O_2 alone, respectively; panels (E and F) represents *f*-MoS_2 samples at 0 day treated with HRP + H_2O_2 and H_2O_2 alone, respectively; panels (G and H) represents *f*-MoS_2 samples at 20 day-treated with HRP + H_2O_2 and H_2O_2 alone, respectively.

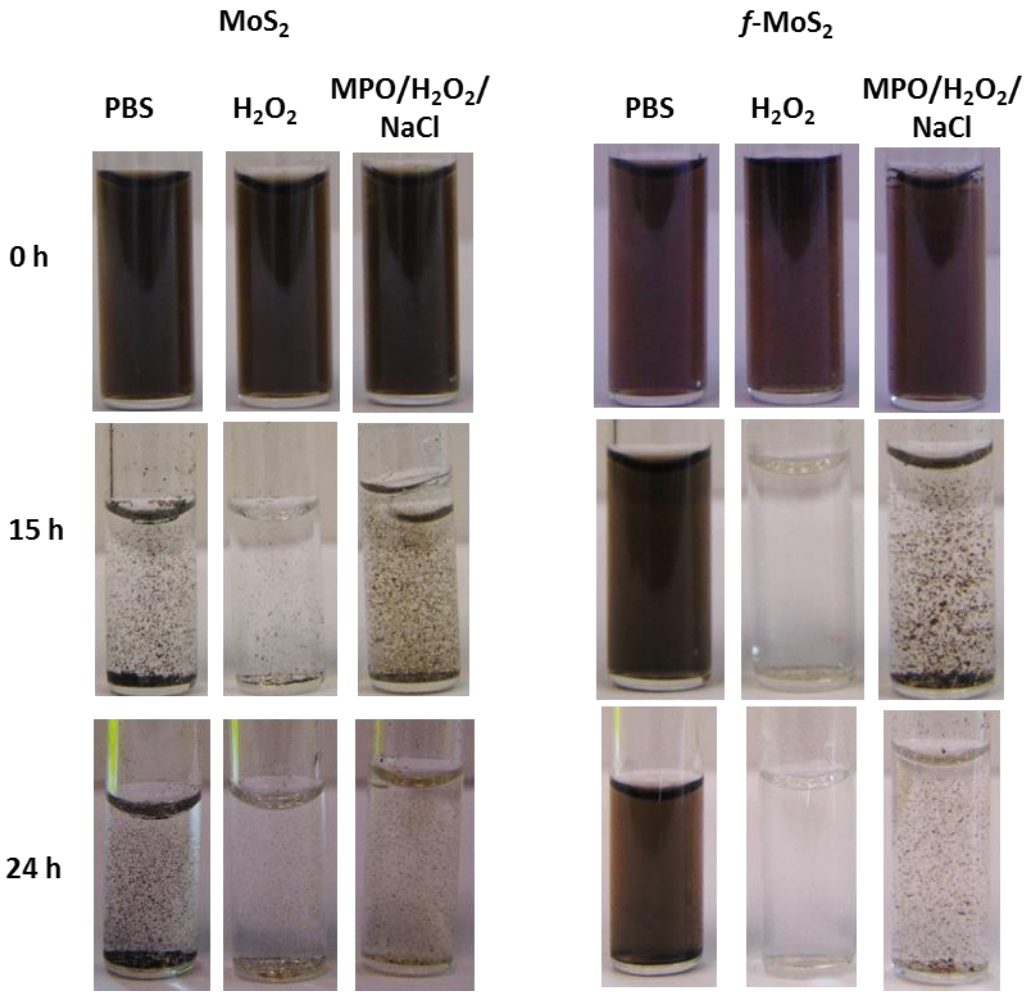

Figure S4: Left side, dispersion images of MoS_2 samples treated with MPO and hydrogen peroxide including the control sample with PBS for 24 h. Right hand side, dispersion images of *f*-MoS_2 samples treated with MPO and hydrogen peroxide including the control sample with PBS. Compared to the pristine MoS_2 sheets *f*-MoS_2 displayed better dispersibility in PBS.

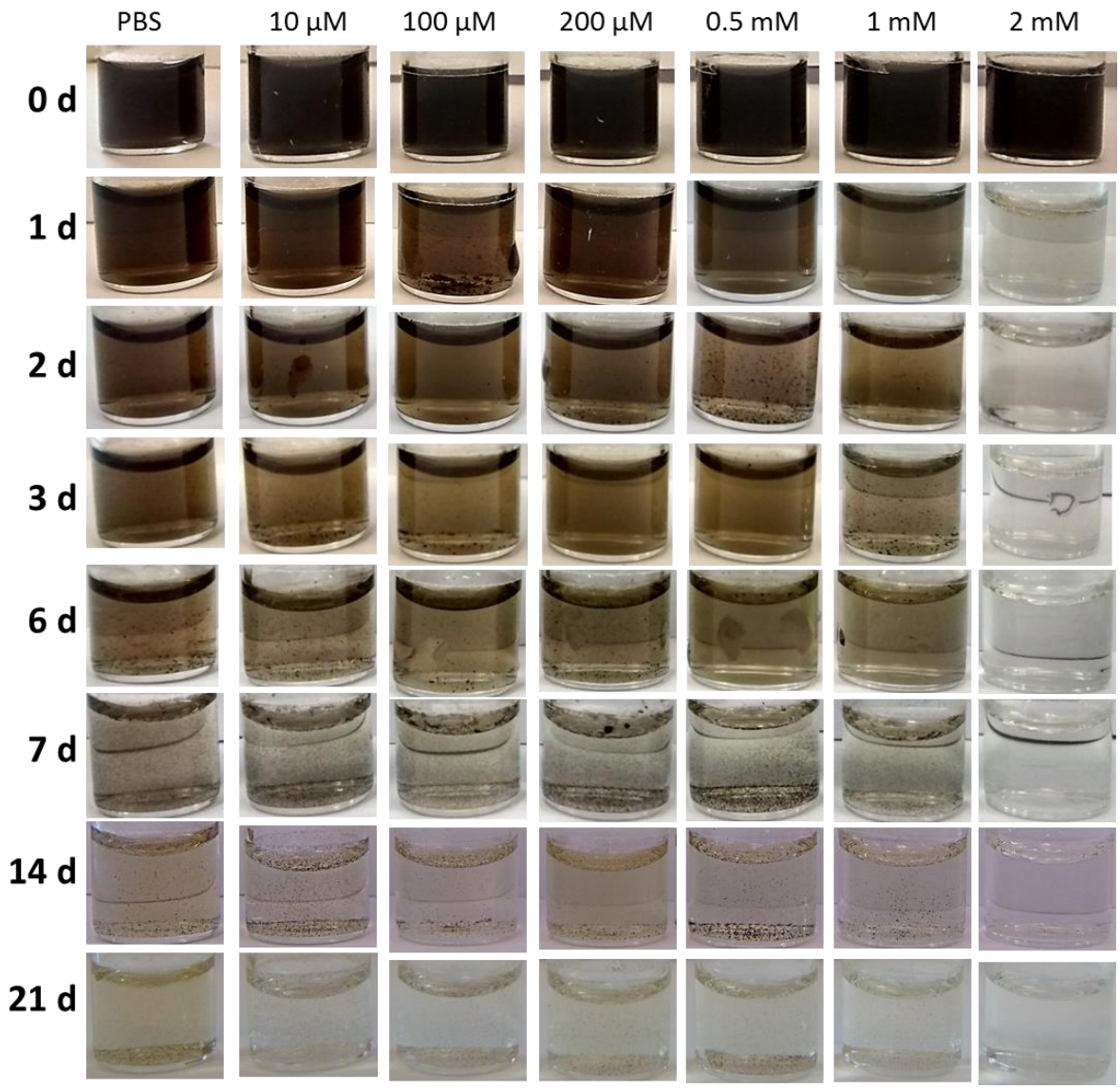

Figure S5: Stability profile of MoS_2 sheets in PBS (control) and hydrogen peroxide starting from 10 µM to 2 mM concentration, added once in a 0 day. The photos of the dispersions were taken at fixed time intervals as shown in the figure.

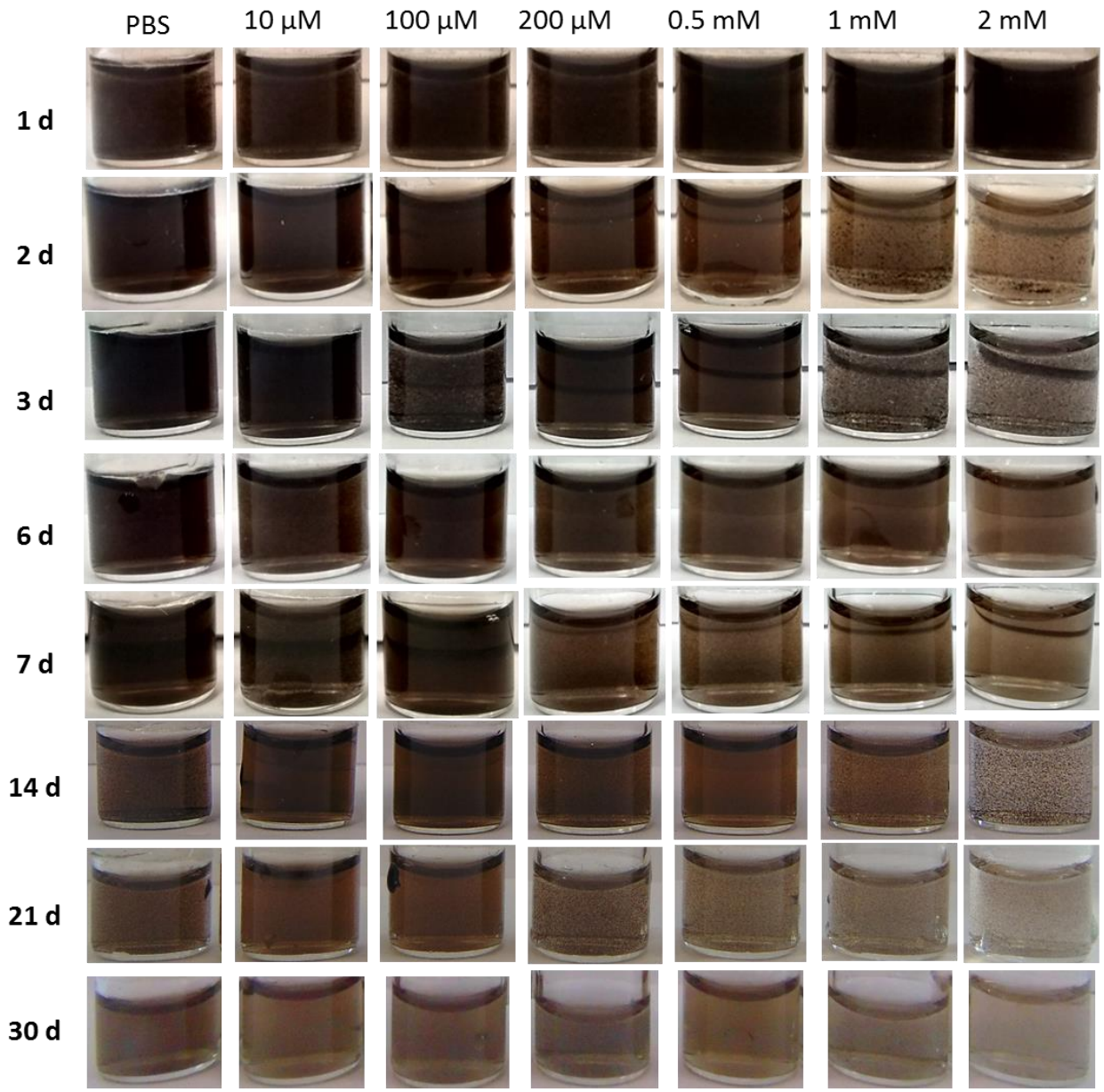

Figure S6: Stability profile of *f*-MoS_2 sheets in PBS (control) and hydrogen peroxide starting from 10 µM to 2 mM concentration, added once in a 0 day. The photos of the dispersions were taken at fixed time intervals as shown in the figure.

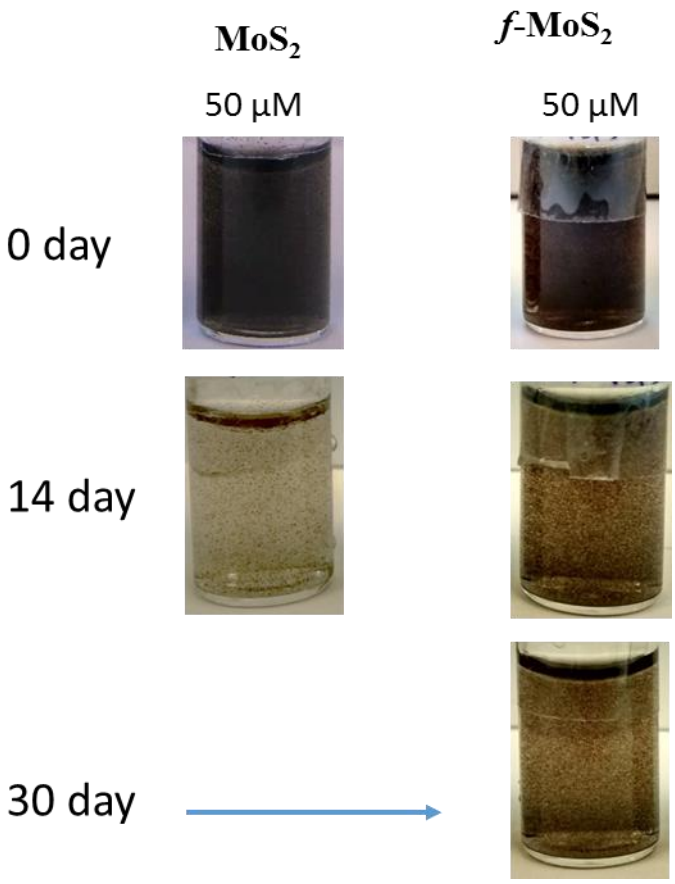

Figure S7: Stability profile of MoS_2 and *f*-MoS_2 sheets in the presence of hydrogen peroxide at 50 µM concentration, added once in a 0 day. The photos of the dispersions were taken at fixed time intervals as shown in the Figure.

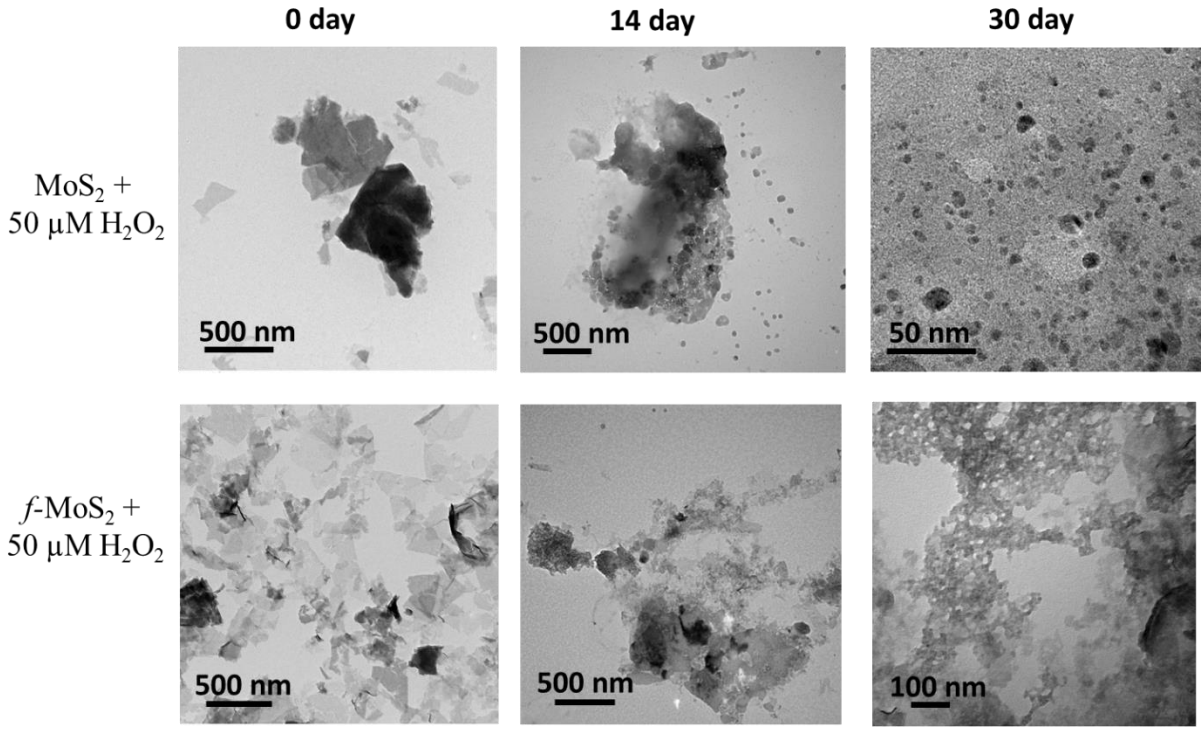

Figure S8: TEM images of MoS_2 (top row) and *f*-MoS_2 (bottom row) sheets after treating with 50 µM of H_2O_2 from 0 to 30 days.

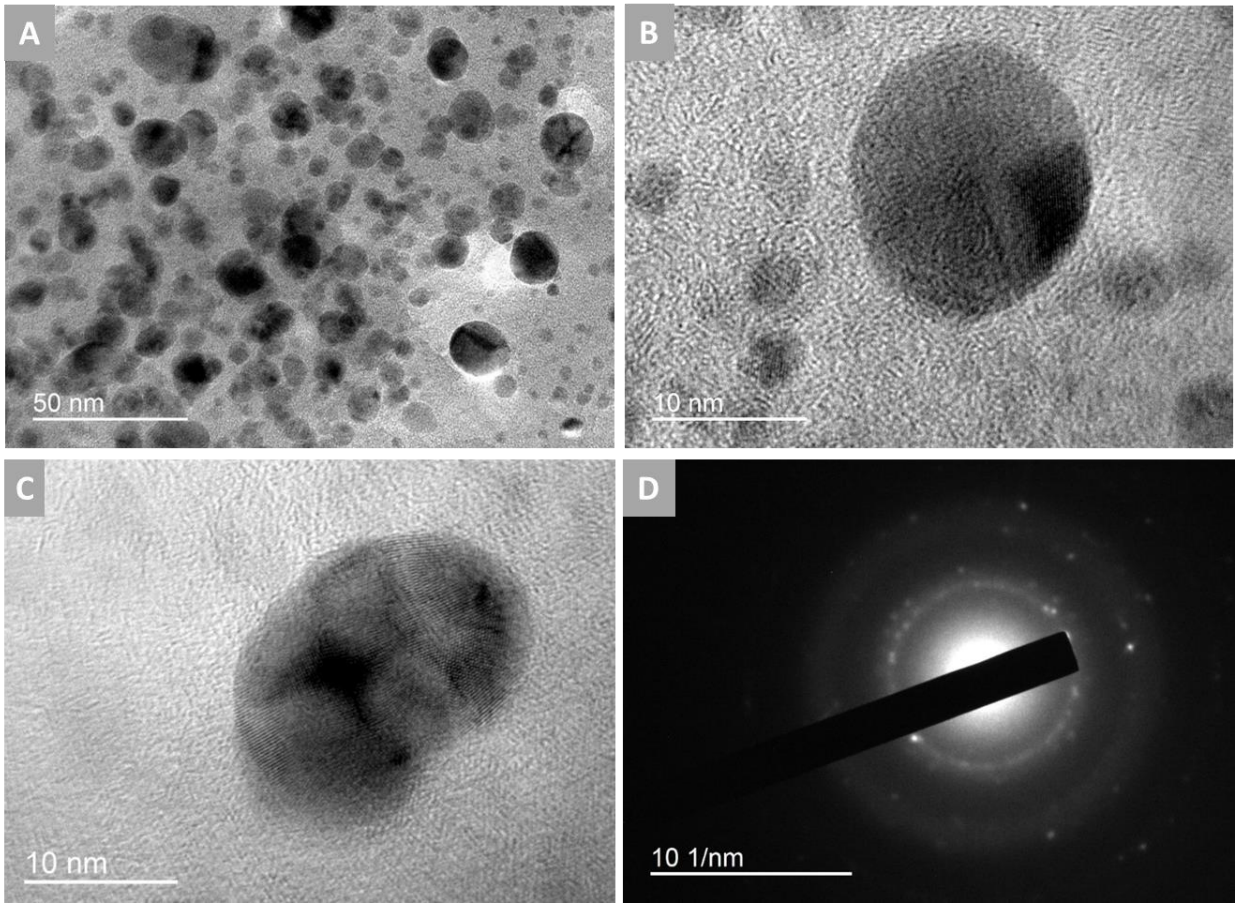

Figure S9: HRTEM images of MoS_2 sheets after treating with 50 µM of H_2O_2 for 30 days. Panels (A) and (B) show the low and high magnification images, respectively; and panel (D) shows SAED pattern of the nanoparticle displayed in (C).

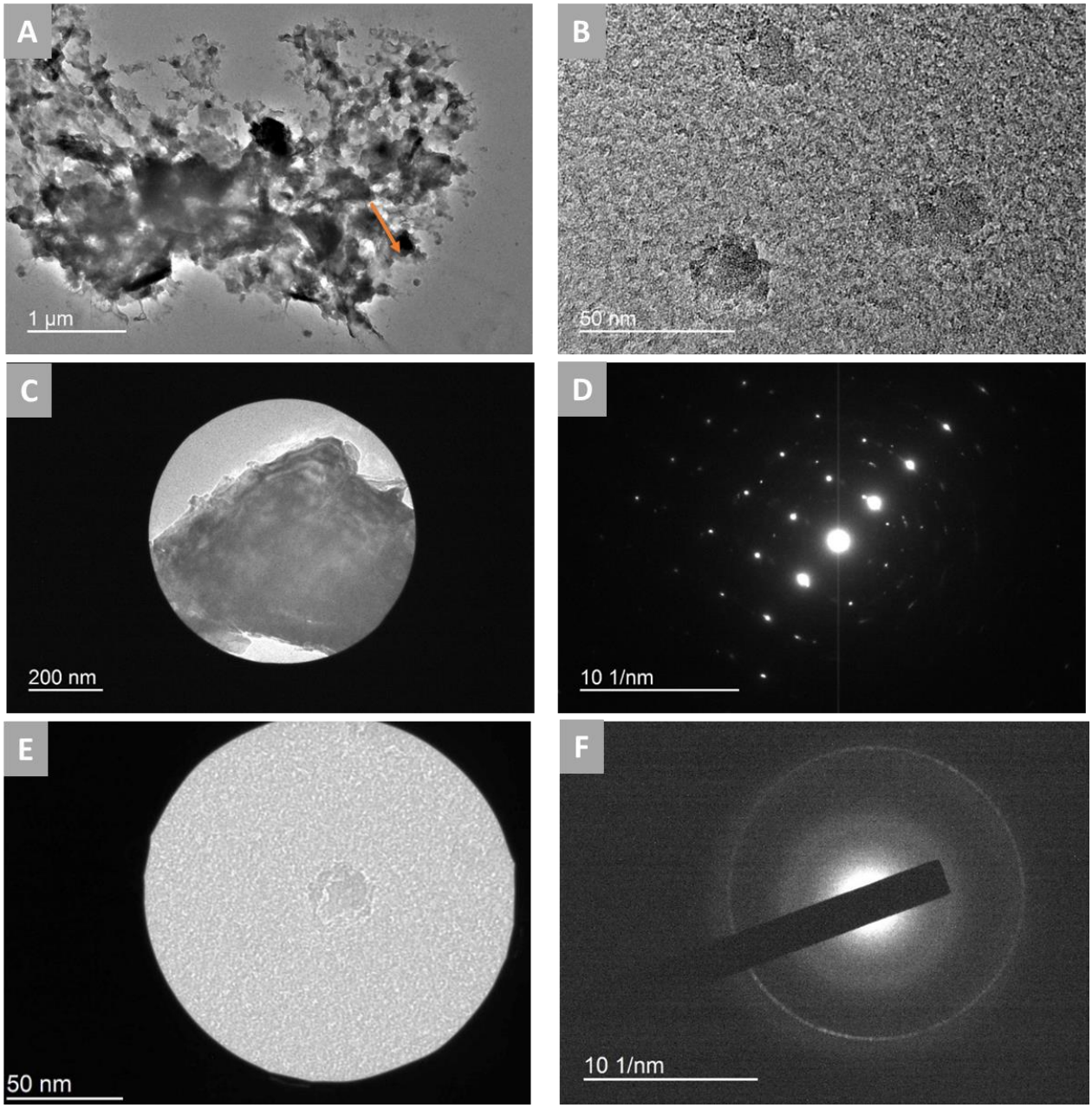

Figure S10: HRTEM images of *f*-MoS_2 sheets after treating with 50 µM of H_2O_2 for (A) 30 days, (B-C and E) 60 days; (D) represents SAED pattern for sheets showed in (C); and (F) represents SAED pattern of the nanoparticle shown in (E).

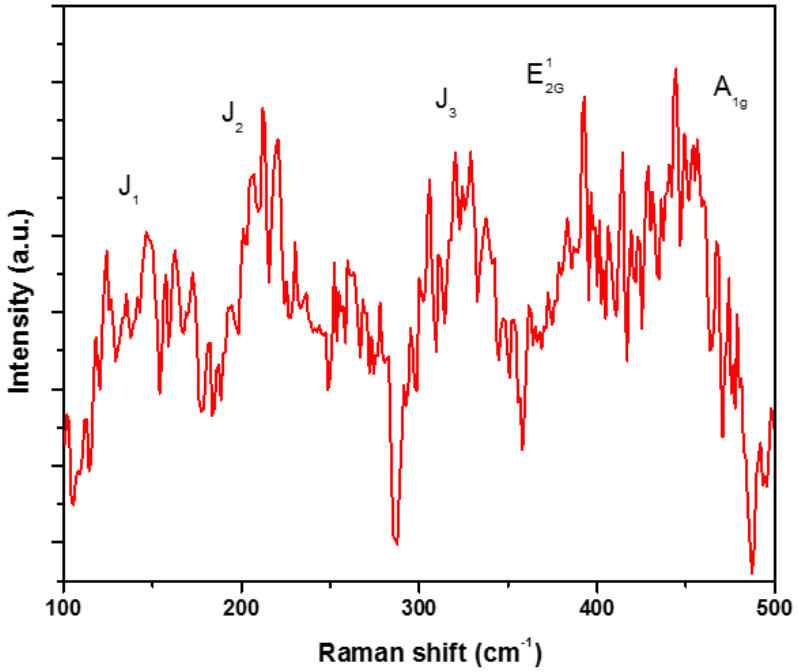

Figure S11: Raman analysis of MPO treated MoS_2 for 24 h after baseline correction.

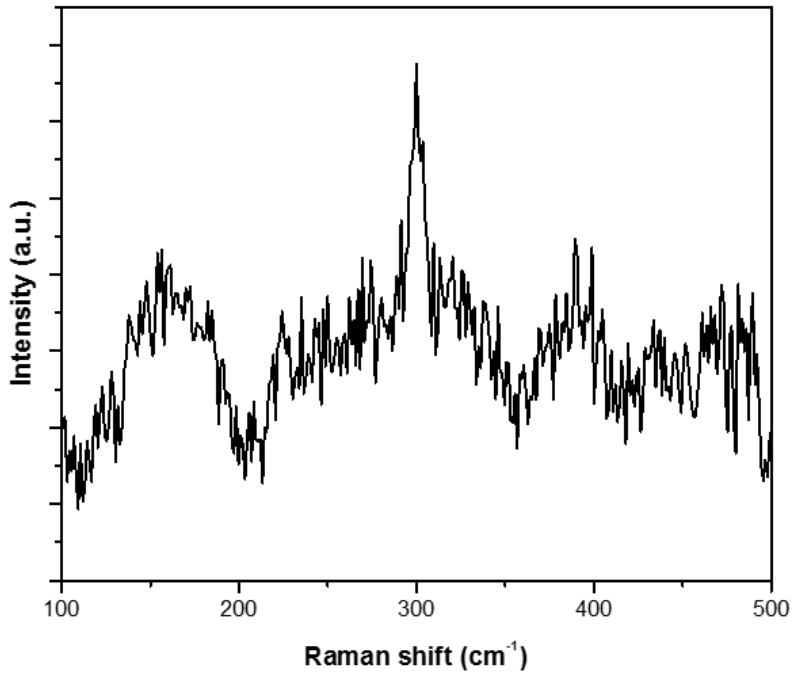

Figure S12: Raman analysis of hMPO treated *f*-MoS_2 for 24 h after baseline correction.

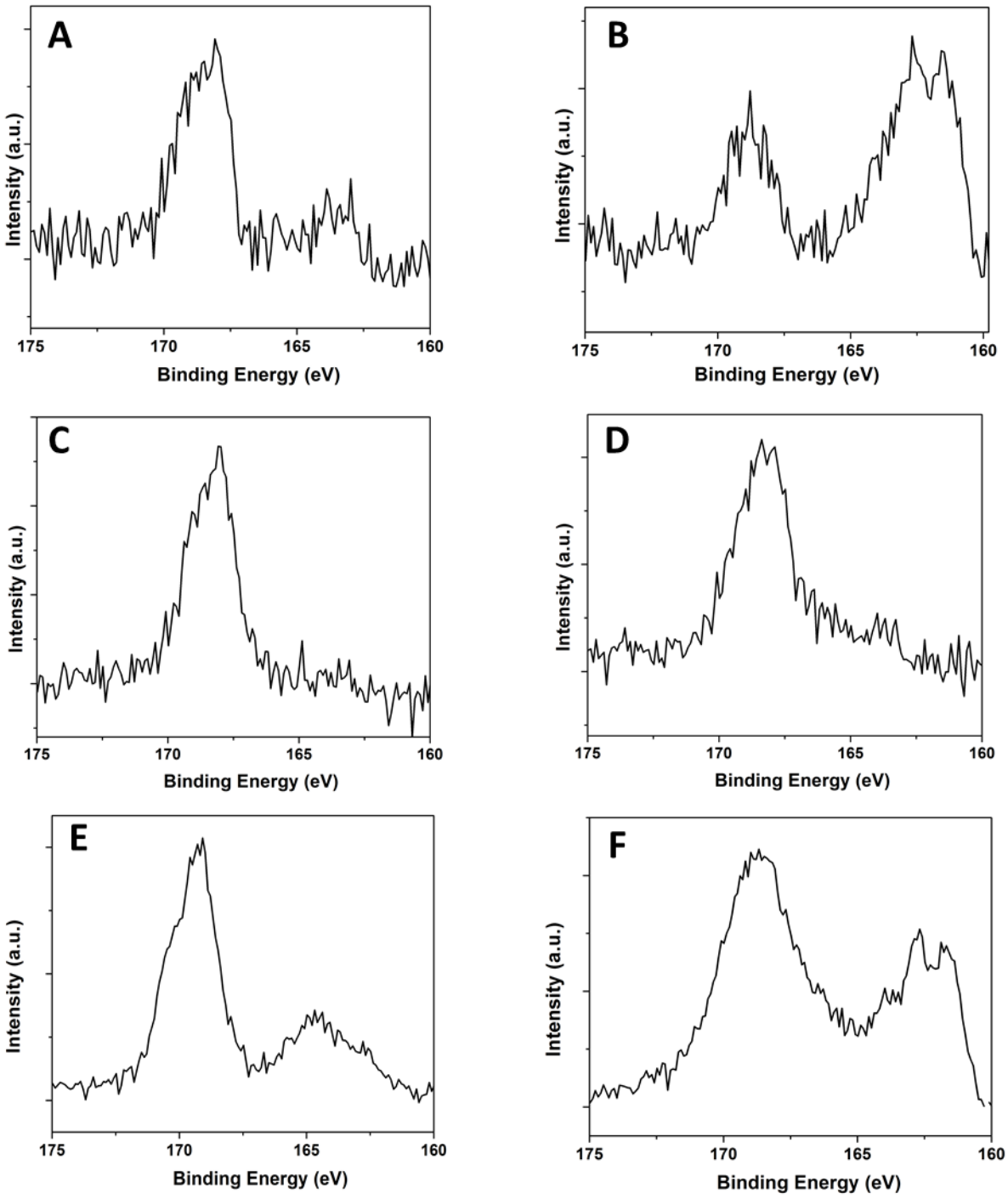

Figure S13: XPS analyses showing high-resolution spectra of S 2p binding energy of MoS_2 and *f*-MoS_2 treated with HRP+H_2O_2 (after 30 d; A & B), MPO+H_2O_2 (after 20 h; C & D), H_2O_2 alone (after 14 for MoS_2 and 30 d for *f*-MoS_2; E & F).

To examine the possibility of a long-term effect, hMDMs were further exposed to 50 μg mL^{-1} of MoS_2 or *f*-MoS_2 for different times and up to 7 days. Cell viability was preserved in all tested time points (Figure S14A). The slight decrease of viable cells after 7 days appears also in control cells and it is due to the normal life cycle of HMDMs.

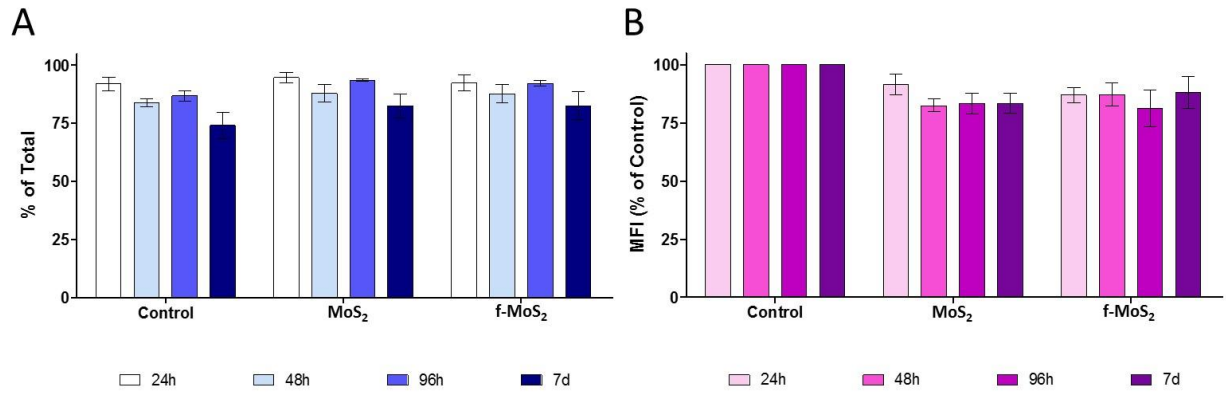

Figure S14: Flow cytometry analysis of hMDM cell viability (A) and cell activation (B) (CD86 expression) after exposure to 50 µg mL^{-1} of MoS_2 or *f*-MoS_2 for different times.

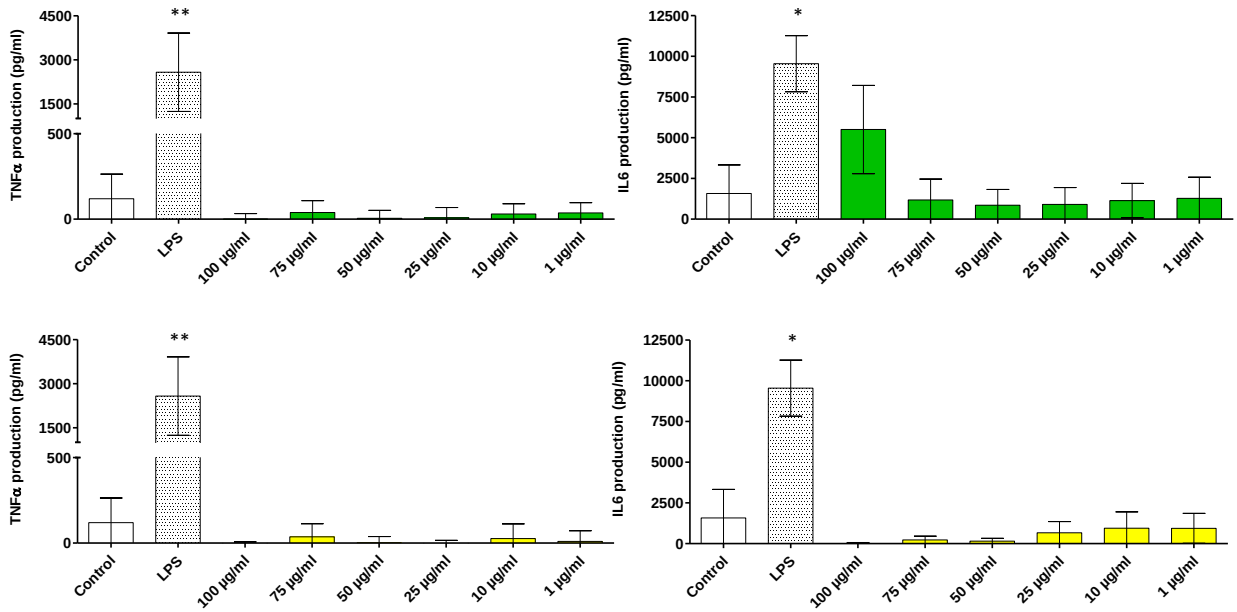

Figure S15: Cytokine production (i.e. TNFα and IL6), determined using ELISA, by hMDMs exposed to increasing concentrations of MoS_2 (top panels) or *f*-MoS_2 (bottom panel) for 24 h. Two-ways ANOVA followed by Bonferroni's post-test was performed to determine the statistical differences versus control cells and to compare MoS_2 and *f*-MoS_2 samples to each other (*p<0.05; **p<0.01; ***p<0.001).

The amount of TNFα secreted by hMDMs exposed to increasing concentrations of MoS_2 or *f*-MoS_2 was comparable to basal levels. A similar situation was found in cells exposed to pristine and *f*-MoS_2 concerning IL6.

The graphs below show the % of live cells after the treatment with buffer solutions containing 50 mM or 100 mM of H_2O_2 for 5 days. The concentrations reported in the graphs are

simulated and represent the composition of the medium during the cell treatment with the MoS_2-DP samples. No effect on cell viability was caused by the buffer MoS_2-DP-free but containing H_2O_2 both in the case of HeLa and RAW 264.7 cells (Figure S16, top and S16, bottom, respectively). The stock solution affected the cells probably because it did not contain complete FBS medium. These data demonstrate that the effects on viability that we have seen in the previous assays are due to MoS_2 degradation products and not to the presence of H_2O_2.

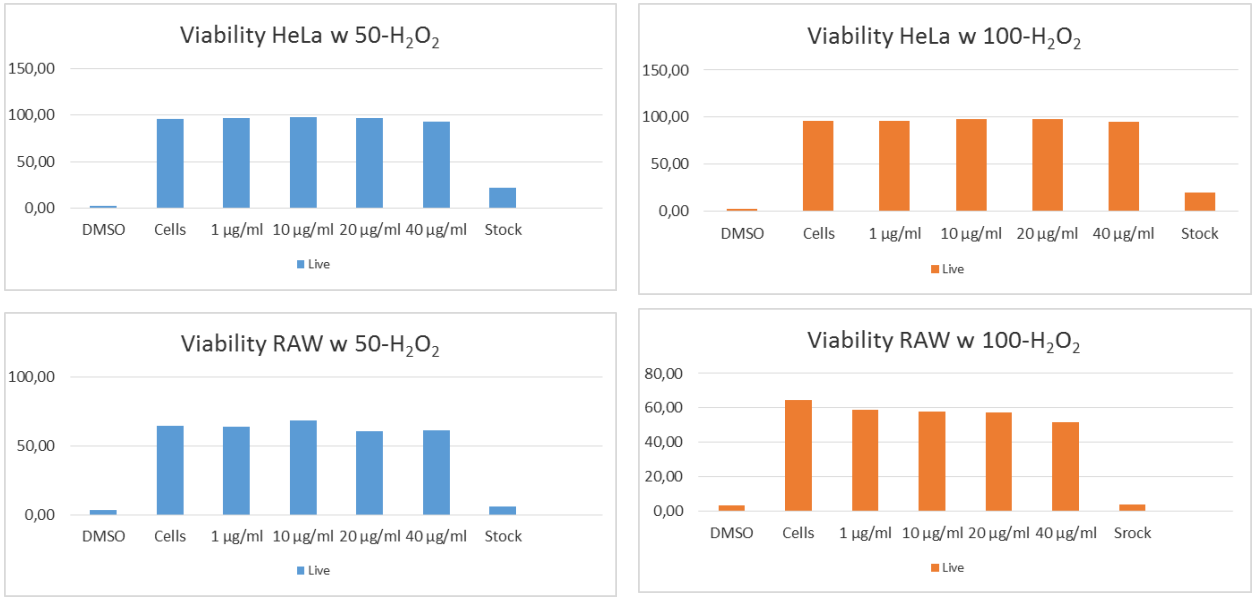

Figure S16. Percentage of HeLa (top) or RAW 264.7 (bottom) live cells after exposure to buffer solutions containing H_2O_2 incubated for 5 days at 37ºC. Analysis was performed by flow cytometry. The concentrations reported in the graphs are simulated and represent the composition of the medium during the cell treatment with the MoS_2-DP samples.

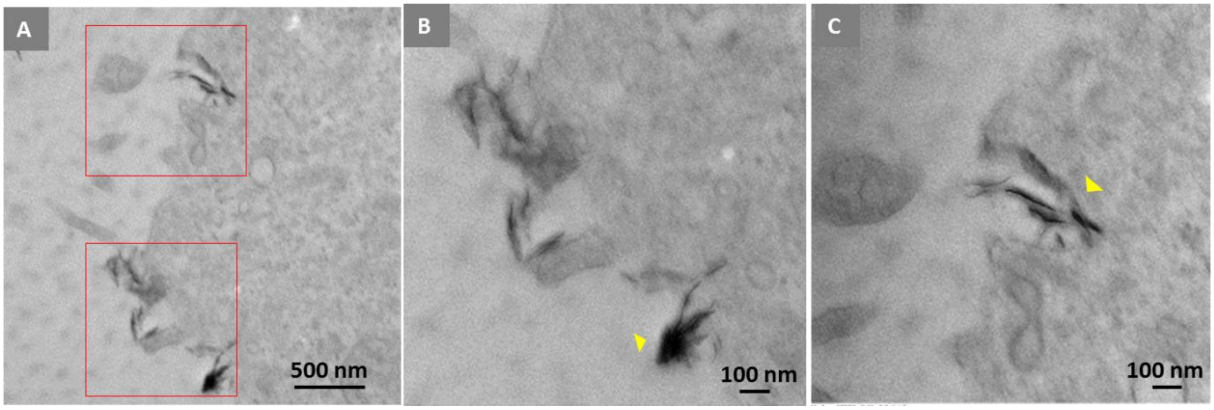

Figure S17. TEM images of HeLa cells incubated with MoS_2 (50 µg mL^{-1}) for 24 h. The red squares in the images are enlarged in the respective closed right panels. Yellow arrows indicate how MoS_2 roll-up and can penetrate as a needle.

References

[1] D. Voiry, A. Goswami, R. Kappera, C. de Carvalho Castro e Silva, D. Kaplan, T. Fujita, M. Chen, T. Asefa, M. Chhowalla, *Nat. Chem.* **2015**, 7, 45.

[2] A. Boyum, *Scand. J. Clin. Lab. Invest.* **1968**, 97, 77.

[3] J. W. Sleasman, L. F. Aleixo, A. Morton, S. Skoda-Smith, M. M. Goodenow, *AIDS* **1996**, 10, 1477.

[4] C. J. Scotton, F. O. Martinez, M. J. Smelt, M. Sironi, M. Locati, A. Mantovani, S. Sozzani, *J. Immunol.* **2005**, 174, 834.

[5] B. Fernandez Pujol, F. C. Lucibello, U. M. Gehling, K. Lindemann, N. Weidner, M. L. Zuzarte, J. Adamkiewicz, H. P. Elsasser, R. Muller, K. Havemann, *Differentiation* **2000**, 65, 287.

[6] J. Melchjorsen, J. Rintahaka, S. Soby, K. A. Horan, A. Poltajainen, L. Ostergaard, S. R. Paludan, S. Matikainen, *J. Virol.* **2010**, 84, 11350.

[7] J.-M. Yun, Y.-J. Noh, C.-H. Lee, S.-I. Na, S. Lee, S. M. Jo, H.-I. Joh, D.-Y. Kim, *Small* **2014**, 10, 2319.

[8] T. K. M. C. K. Gupta, *Hydrometallurgy in Extraction Processes*, Vol. 2, CRC Press, 1990.